Gondwana Research 26 (2014) 594–607

Contents lists available at ScienceDirect

Gondwana Research

journal homepage: www.elsevier.com/locate/gr

Microscale sulfur isotopic compositions of sulfide minerals from the Jinding Zn–Pb deposit, Yunnan Province, Southwest China ☆

Yong-Yong Tang [a,b], Xian-Wu Bi [a,*], Mostafa Fayek [c], Rui-Zhong Hu [a], Li-Yan Wu [a], Zhi-Chao Zou [a,b], Cai-Xia Feng [a], Xin-Song Wang [a,b]

[a] State Key Laboratory of Ore Deposit Geochemistry, Institute of Geochemistry, Chinese Academy of Sciences, Guiyang 550002, China
[b] University of Chinese Academy of Sciences, Beijing 100049, China
[c] Department of Geological Sciences, University of Manitoba, Winnipeg, MB R3T 2N2, Canada

ARTICLE INFO

Article history:
Received 8 March 2013
Received in revised form 19 July 2013
Accepted 23 July 2013
Available online 25 August 2013

Keywords:
Sulfur isotopes
Sulfide minerals
Jinding
Zn–Pb deposit
Southwest China

ABSTRACT

The Jinding Zn–Pb deposit, located in the Lanping basin in Northwest Yunnan Province, is the largest Zn–Pb deposit in China, and also probably the youngest sediment-hosted super giant Zn–Pb deposit in the world. Its genesis differs from the well-known major types of sediment-hosted Zn–Pb deposits. Based on mineral paragenesis and textures, there are two stages of mineralization: stage 1 that is typically characterized by fine-grained sulfide minerals (galena, sphalerite, pyrite and marcasite) disseminated in sandstones of the Lower Cretaceous Jingxing Formation (K_1j), and massive sulfides in limestone breccias of the Paleocene Yunlong Formation (E_1y); and stage 2 which mainly occurs as coarse-grained galena veins crosscutting stage 1 sulfides, and minor amounts of colloform sphalerite intergrown with galena. In situ sulfur isotopic analyses of galena, sphalerite and pyrite were determined by secondary ion mass spectrometry (SIMS), and showed highly variable $\delta^{34}S$ values (−42.1‰–7.7‰) of different ore types. Stage 1 mineralization has $\delta^{34}S$ values from −42.1‰ to −10.2‰ with the majority ranging from −26‰ to −14‰. Stage 2 mineralization has higher $\delta^{34}S$ values (−8.3‰–7.7‰). Combined with the geological settings and mineral paragenesis, the sulfur isotopic data presented here suggest multiple sulfur sources (biogenic sulfur + evaporites) and formation mechanisms for reduced sulfur (H_2S). H_2S responsible for stage 1 sulfide precipitation was associated with bacterial sulfate reduction (BSR). However, H_2S of stage 2 was likely derived from thermochemical sulfate reduction (TSR). The most reasonable scenario for the stage 1 mineralization is a metal-bearing brine mixing with an H_2S-rich fluid, thereby causing rapid sulfide precipitation. Till the stage 2, the ore-forming fluid shifted to the meteoric water that infiltrated and reacted with evaporitic rocks, leached metals and transported them as sulfate- or sulfite-complexes to the Jinding dome where the oxidized sulfur was reduced by organic matters to H_2S, leading to precipitation of metal sulfides. In contrast to other sulfide deposits in the Lanping basin, biogenic sulfur might have played a key role in the mineralization process, especially during the early stage of formation of the Jinding Zn–Pb deposit.

1. Introduction

Numerous sediment-hosted base metal deposits are located in the Tuotuohe, Yushu, Changdu, and Lanping basins in the Sangjiang area along the northeastern margin of Tibetan plateau, Southwest China. Particularly in the Lanping basin, there are a lot of significant economic sediment-hosted Zn–Pb–Cu–Ag deposits, like the Jinding super giant Zn–Pb deposit (Shi et al., 1983; Qin and Zhu, 1991; Luo et al., 1994; Li and Kyle, 1997; Kyle and Li, 2002; Xue et al., 2007a; Tang et al., 2011), the Baiyangping Zn–Pb–Ag–Cu concentrated district (Chen et al., 2000; Gong et al., 2000; Yang et al., 2003; Liu et al., 2010; Feng et al., 2011), and the Jinman Cu deposit (Yan and Li, 1997; Ji and Li, 1998; Liu et al., 2001; Gao et al., 2006; Zhang and Wen, 2012) (Fig. 1). These deposits formed in the highly deformed Paleogene foreland basin within an active collisional setting (Hou et al., 2006, 2007; Xue et al., 2007a; Hou and Cook, 2009). The emplacement of these sulfide deposits is strictly constrained by the Cenozoic thrust fault systems related to Indo-Asian continental collision (Xu and Li, 2003; L.Q. He et al., 2004; Xu and Zhou, 2004). These large thrust nappe-controlling sediment-hosted base metal deposits in the compressional regime distinguish from the major types of sediment-hosted base metal deposits recognized in the world, including Sedimentary Exhalative-type (SEDEX) Zn–Pb deposits, Mississippi Valley-type (MVT) Zn–Pb deposits, Sandstone-type (SST) Pb–Zn deposits and Sandstone-type (SSC) Cu deposits (Misra, 2000; Leach et al., 2005; He et al., 2009; Wang et al., 2009). The SEDEX deposits are generally considered to form in the continental rifting environments (Basuki and Spooner, 2004), in contrast to the

☆ This article belongs to the Special Issue on Orogenesis and metallogenesis in the Sanjiang Tethyan Domain.

* Corresponding author. Tel.: +86 851 5891 962 (office).
E-mail address: bixianwu@vip.gyig.ac.cn (X.-W. Bi).

1342-937X/$ – see front matter © 2013 International Association for Gondwana Research. Published by Elsevier B.V. All rights reserved.
http://dx.doi.org/10.1016/j.gr.2013.07.021

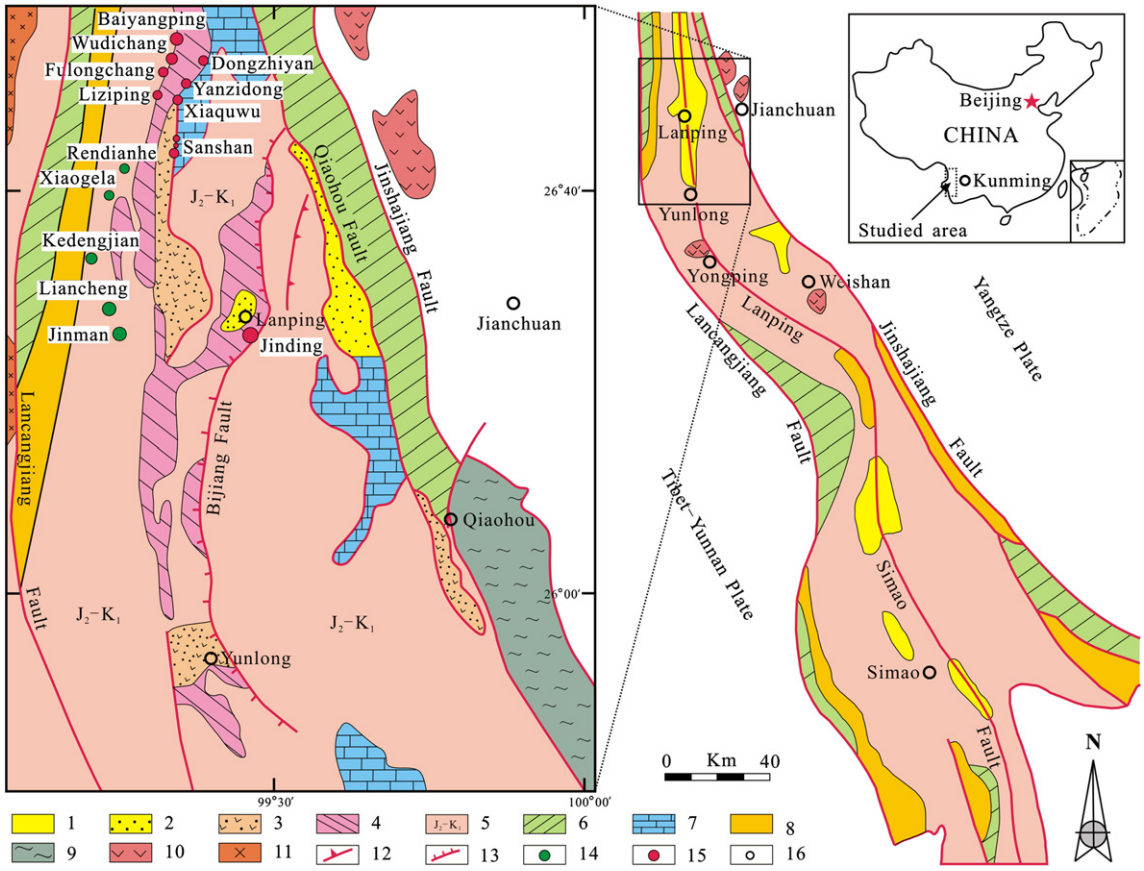

Fig. 1. Sketch geological map of the Lanping–Simao basin in western Yunnan, China, with enlargement of the Lanping basin showing the main mineralized zones. 1—Cenozoic clastic rocks. 2—Miocene sandstone, mudstone and conglomerates. 3—Eocene–Oligocene sandstone and conglomerates. 4—Paleocene Yunlong Formation. 5—Middle Jurassic–Lower Cretaceous silisic clasts. 6—Middle–Upper Triassic volcanics, silisic clasts and carbonate. 7—Upper Triassic limestones. 8—Paleozoic metamorphic flysch. 9—Precambrin–Devonian metamorphic rocks. 10—Neogene alkali rocks and trachytes. 11—Yanshanian diorites and quartz diorites. 12—Overthrusting fault. 13—Growth fault. 14—Cu mineralized zone. 15—Pb–Zn mineralized zone. 16—City. Modified after Zhao (2006) and Xue et al. (2007a).

MVT deposits that usually occur in the orogenic foreland basins (Bradley and Leach, 2003) or intracontinental rifting basins (Clendenin and Duane, 1990; Sangster, 1990). The SST deposits are hosted in mature marine quartz-rich sandstones in prolonged stable geological settings (Bjorlykke and Sangster, 1981), whereas, the SSC deposits form within the red sandstones (Misra, 2000). Therefore, studies of the Zn–Pb–Cu–Ag deposits in southwestern China provide good opportunities to study the base-metal ore-forming systems in the continental collisional orogenic settings (He et al., 2009).

The Jinding deposit is the largest Zn–Pb deposit in China, and also probably the youngest sediment-hosted super giant Zn–Pb deposit in the world (Xue et al., 2000, 2007a; Khin et al., 2007). It consists of approximately 220 Mt base metals, covering a surface area of about 8 km^2 (Third Geological Team, 1984), which were estimated about 317×10^4 m^3 reduced sulfur (H_2S) involved in the mineralization (Gao et al., 2008). The deposit, hosted in the siliciclastic strata of Early Cretaceous and Paleocene, is characterized by simple mineralogy, fine-grained ore textures and involvement of basinal brines in the mineralization (Qin and Zhu, 1991; Li, 1998; Kyle and Li, 2002; Chi et al., 2007). The genesis of the deposit has been a subject of debate and controversy since the 1980s. Previous studies have proposed two contrasting genetic models: (1) syngenetic origin with the emphasis on the mineralization during the synsedimentary period (Shi et al., 1983; Bai et al., 1985; Zhao, 1989; Qin and Zhu, 1991; Luo et al., 1994; Hu et al., 1998), and (2) epigenetic origin focusing on late hydrothermal superimposition or modification (Gao, 1989; Hu, 1989a; Li and Kyle, 1997; Kyle and Li, 2002; Xue et al., 2007a). These studies used the conventional bulk-grain analytical techniques for sulfur isotopic analysis and reported $\delta^{34}S_{V\text{-}CDT}$ values of sulfide minerals from the Jinding Zn–Pb deposit that ranged from −30.4‰ to −1.8‰. Based on these values, Zhao (1989), and Zhou and Zhou (1992) suggested multiple sulfur sources of evaporites and mantle-derived sulfur. However, Ye et al. (1992), Xue et al. (2002) and Gao et al. (2008) suggested that the source of sulfur was evaporites in the Lanping basin, and reduced sulfur might be derived from bacterial sulfate reduction (BSR) and thermochemical sulfate reduction (TSR). Because sampling techniques such as microdrilling or mineral separation greatly exceeds the scale of texture variations (μm) in sulfide minerals, it is difficult to obtain pure minerals of the same generation for sulfur isotopic analysis by classical methods. Therefore, previously reported $\delta^{34}S$ values of sulfides from the Jinding deposit likely represented average values of different mineralization stages, which made the sources of the sulfur and mechanisms of sulfide precipitation, difficult to interpret.

While analysis of mg-quantities of material is routine for both stable and radiogenic isotopic analyses, important geologic features such as zoned minerals and micro-scale alteration phases require in situ measurements at the micron scale (e.g., Reed, 1990; Neal et al., 1995). The secondary ion mass spectrometry (SIMS) is capable of performing in situ measurements with ca. 10 μm resolution and progress has been made in developing precise and accurate methods for the isotopic analysis using this instrument (McKeegan, 1987; Reed, 1989; Neal et al., 1995; Riciputi et al., 1998; Ireland, 2004; Kozdon et al., 2010). Many studies have shown unique advantages of in situ analysis for sulfur isotopes of microscale intracrystals in understanding the detailed mineralizing processes that cannot be resolved from bulk $\delta^{34}S$ values (Deloule et al., 1986; Layne et al., 1991; McKibben and Eldridge, 1995; Peevler et al., 2003; Ferrini et al., 2010; Drake et al., 2013). However, SIMS was chosen in this study to determine in situ sulfur isotopes of sulfide

minerals from different mineralization stages of the Jinding Zn–Pb deposit, which could effectively avoid mixed sulfur isotopic information introduced by the conventional sulfur isotopic analysis used before. In situ measurements of sulfur isotope enable us to discuss the sources of sulfur and formation mechanisms of reduced sulfur of different mineralization stages, and finally conclude the genetic history of the Jinding deposit.

2. Geological settings

2.1. Regional geology

The Sanjiang area, defined by the Jinshajiang–Ailaoshan, Lancangjiang and Nujiang shear zones in the southwestern China, has experienced the multi-episodes of ocean–continental subduction in the Tethys Period and the continental–continental collision in Cenozoic; various ore deposits formed in the ocean growth and subduction environment, as well as the transition stage from the main collision to late collision, and Cenozoic collision induced the formation of porphyry Cu–Au deposits, sediment-hosted Pb–Zn–Ag–Cu deposits and orogenic Au deposits (Deng et al., 2010, 2012).

The Lanping–Simao basin, known as part of Sanjiang fold-and-thrust belt, is a north–northwest-trending intracontinental basin developed on the Changdu–Lanping–Simao microplate between the Tibet–Yunnan plate west of the Lancangjiang fault and the Yangtze plate east of the Jinshajiang–Ailaoshan fault (Fig. 1) (Yin et al., 1990). The Yangtze plate, Tibet–Yunnan plate and the Changdu–Lanping–Simao microplate initially departed from Gondwana and collaged to Eurasia during the Late Paleozoic and Early Mesozoic (Sengor, 1985; Chen et al., 1995; Scotese, 2000; Veevers, 2006, 2009; Metcalfe, 2011; Yu et al., 2012; Lehmann et al., 2013). In the Late Paleozoic, the Changdu–Lanping–Simao microplate was separated by oceans (Jinshajiang Paleo-Tethyan Ocean to the east and Lancangjiang Paleo-Tethyan Ocean to the west) from the Yangtze plate and Tibet–Yunnan plate (Feng, 2002; Tao et al., 2002; Metcalfe, 2006; Xue et al., 2007a; Jian et al., 2009; Metcalfe, 2011). When the Paleo-Tethyan Ocean was closed in the Late Permian or Early Triassic, the Lancangjiang and Jinshajiang oceanic plates subducted eastward and westward beneath the microplate, respectively, leading to a conjunction of the Yangtze plate, Tibet–Yunnan plate and the clamping microplate (Luo et al., 1994; Jin et al., 2003). Then, the Lanping–Simao basin, based on the Paleo-Tethyan basement, started an intracontinental evolution which approximately included Late Triassic rifting, Jurassic–Cretaceous depression, and Paleogene foreland basin (Yin and Harrison, 2000; Wang et al., 2001; Spurlin et al., 2005; Li et al., 2006; He et al., 2009).

The metamorphic basement of the Lanping–Simao basin consists of Proterozoic and Paleozoic strata, which are mainly distributed along the margins of the basin (Xue et al., 2007a). Inside the basin, it was

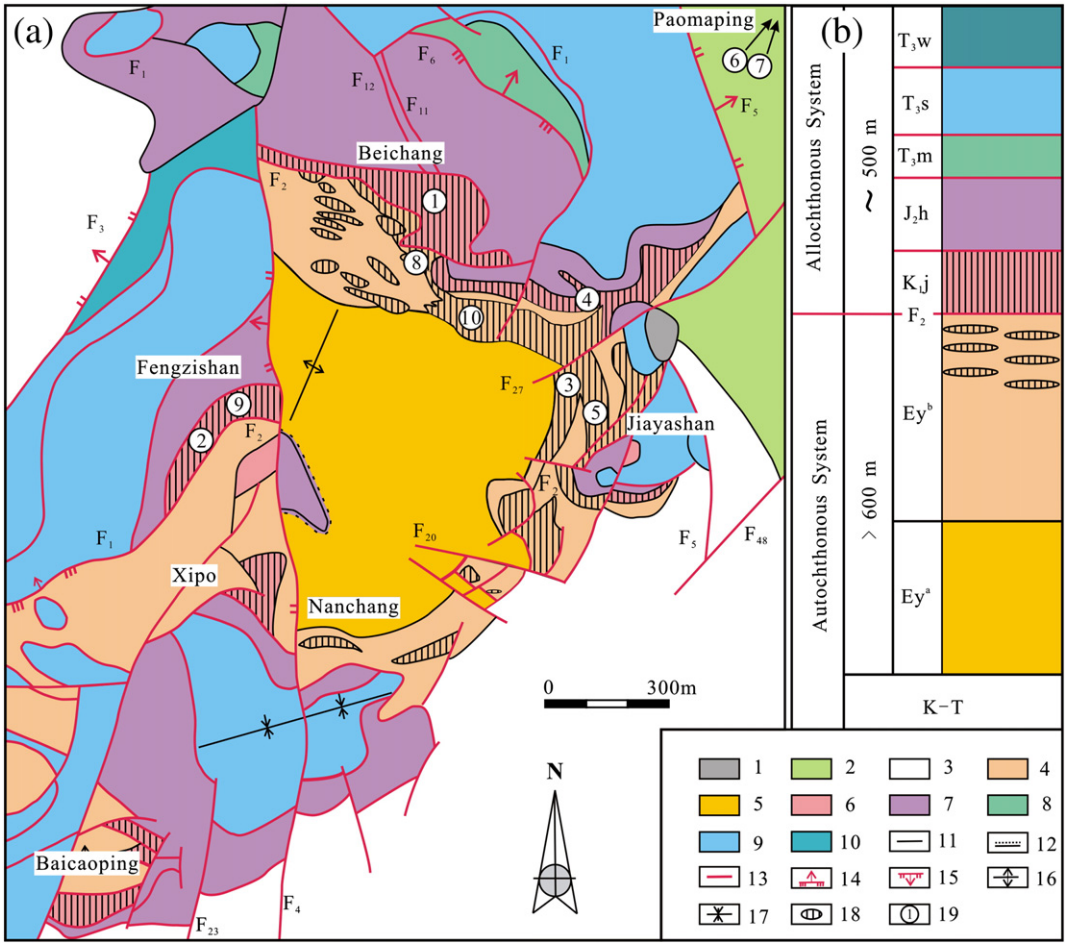

Fig. 2. (a) Map of the geology and structures associated with the Jinding Zn–Pb deposit (Third Geological Team, 1984) and (b) schematic stratigraphic column in the Jinding deposit. 1—Pleistocene gravel and sand (QP). 2—Paleocene Guolang Formation (Eg), muddy siltstone intergrown with fine sandstone. 3—Paleocene Yunlong Formation (Ey^2), conglomerates entraining gypsum and siltstone. 4—Paleocene Yunlong Formation (Ey^b), gypsum-bearing limestone breccia and siltstone. 5—Paleocene Yunlong Formation (Ey^a), fine sandstone and siltstone containing limestone blocks. 6—Lower Cretaceous Jingxing Formation (K_1j), sandstone and sandy limestone breccia. 7—Middle Jurassic Huakaizuo Formation (J_2h), silty mudstone, siltstone and fine sandstone. 8—Upper Triassic Maichuqing Formation (T_3m), silty mudstone. 9—Upper Triassic Sanhedong Formation (T_3s), calcareous mudstone, firestone- or bitumen-bearing dolomitic limestone. 10—Upper Triassic Waigucun Formation (T_3w), muddy siltstone. 11—Geological boundary. 12—Unconformable boundary. 13—Ambiguous fault. 14—Thrust fault. 15—Normal fault. 16—Anticline axes. 17—Syncline axes. 18—Zn–Pb ores. 19—Sample location.

mainly filled with the Mesozoic–Cenozoic strata, comprising Late Triassic marine clastics, carbonates and sandy mudstones, Jurassic marine–terrestrial red clastics and minor carbonates, Cretaceous shallow lake-facies red clastics, and Cenozoic siliciclastics (Mu et al., 1999; Zhong et al., 2000; Liao and Chen, 2005). At least six horizons of evaporites, dominated by gypsum with minor halite, and occasionally also sylvite, with a local total thickness of over 2 km, have mainly been recognized in Middle–Upper Triassic, Middle–Upper Jurassic and Paleocene sediments (Gao, 1989; Xue et al., 2007a; He et al., 2009).

Over 100 Pb–Zn–Ag–Cu deposits or occurrences are located in the Lanping basin, most of which are concentrated in the northern segment of the basin and spatially classified into four ore belts (Jinman Cu belt, Baiyangping Pb–Zn–Ag–Cu belt, Sanshan Pb–Zn belt and Jinding Zn–Pb deposit) (Hou et al., 2006; He et al., 2009). These deposits are commonly hosted in the Mesozoic–Cenozoic siliciclastics, and controlled by the Cenozoic thrust fault structures (Wang et al., 2001; Hou et al., 2006, 2008). Besides, the local continental crust uplifting, associated with India–Eurasian continental collisional compression, might produce the dome structure which provided favorable space for metal precipitation (Xue et al., 2002). Cenozoic magmatic rocks (68–23 Ma) are dominantly exposed along the margins of the basin, except a few outcrops inside the basin (e.g., Zhuopan intrusives in Yongping County) (Zhang et al., 2000; Hou et al., 2003; Xue et al., 2003; Liu et al., 2006).

2.2. Deposit-scale geology

The Jinding Zn–Pb deposit, consisting of Paomaping, Beichang, Jiayashan, Fengzishan, Nanchang, Xipo and Baicaoping ore blocks (Fig. 2a), is located at the eastern wing of Gaoping–Laomujing syncline and to the west of Pijiang fault (part of the Lanping–Simao fault, Luo et al., 1994). The strata include rocks of both the autochthonous and the overlying allochthonous systems as a result of regional westward over-thrusting. The allochthonous system containing Upper Triassic Waigucun, Sanhedong and Maichuqing Formations, Middle Jurassic Huakaizuo Formation and Lower Cretaceous Jingxing Formation, is juxtaposed over the autochthonous system consisting of Paleocene Yunlong Formation and the Mesozoic strata (Fig. 2b). The Jinding deposit is hosted within a tectonic dome, approximately 3 km long and 2.5 km wide with a NNE-trending axis. The autochthon comprises the core of the dome, and is surrounded by the allochthon. Two systems are separated by the overthrust fault (F_2). Sulfide ores, chiefly occurring as sheet-like, stratoid or lenticular ores controlled by lithofacies and structures, are hosted in the limestone breccias of Paleocene Yunlong Formation and the overlying sandstones of Early Cretaceous Jingxing Formation (Fig. 3) (Third Geological Team, 1984; Luo et al., 1994). Abundant sulfates (such as gypsum, celestite and barite) discontinuously occur in the vicinity of the sulfide ores. Organic matters are wide-spread in the ore field, and occur as bitumen and fossil oil fillings in the fractures and dissolution cavities of ores, and organic fluid inclusions discovered in transparent and non-transparent minerals (Fu, 2004; Xue et al., 2007a). Hu (1989b) reported that both ore-bearing strata and non ore-bearing strata (Triassic limestones) in the Jinding deposit showed much higher contents of organic matters (mean 3.55% and 1.99%, respectively) than similar sediments (<0.5% for carbonate rocks, and 0.05% for sandstones) in regional area.

The deposit has had a complex fluid history. However, sulfide mineralization can be grouped into two stages based on mineral paragenesis and textures (Fig. 4).

Stage 1 mineralization Stage 1 sulfides can be further subdivided into two sub-types: (1) fine-grained disseminated in sandstones and (2) massive or as veins in limestone breccias. The relationship between these two sub-types is difficult to distinguish, because they are hosted in different rock units, (1) within the upper ore-bearing layer of Lower Cretaceous Jingxing Formation quartz sandstones and (2) within the lower counterpart of Paleocene Yunlong Formation limestone breccias. Stage 1 is characterized by extensive Zn mineralization. The (1) sub-type ores display quartz, feldspar and calcite, sphalerite, pyrite (sometime marcasite), and galena as dominant mineral components (Figs. 5a, 6a, b). Sulfide minerals occur as fine-grained (0.05–0.03 mm) disseminated mineralization, together with diagenetic calcite cements, detrital quartz and feldspar. The (2) sub-type ores are characterized by a simple mineral assemblage of sphalerite, galena, pyrite and calcite hosted in limestone breccias (Fig. 5b, c, e).

Stage 2 mineralization This stage of mineralization is mainly characterized by the late coarse-grained galena veins (up to 3 cm in width) crosscutting stage 1 sulfide mineralization (Figs. 5e, 6c, f), and, minor colloform sphalerite intergrown with vein galena hosted by limestone breccias (Figs. 5f, 6g). Colloform sphalerite shows concentric ring structures and is surrounded by galena. This texture is similar to sulfides that were interpreted to have formed from late metal-rich colloidal solution (Third Geological Team, 1984; Zhao, 2006; Zeng, 2007). Barite occurs with stage 2 galena (Fig. 6d, f).

3. Samples and analytical methods

Ten polished thin sections were prepared from hand specimens sampled from Paomaping, Beichang, Jiayashan and Fengzishan districts. Mineralogical and textural relationships within the samples were characterized using both optical and scanning electron microscopy (SEM). Thin sections were examined in transmitted and reflected light using a polarizing microscope. Then, these sections were carbon coated, to create a conductive surface, prior to analysis using a Cambridge Stereoscan 120 scanning electron microscope (SEM) at the University of Manitoba (Canada). The SEM is equipped with a back-scattered electron detector as well as an energy dispersive X-ray spectroscopy detector which was used to further characterize the textures present within the samples and for qualitative chemical characterization of the minerals. The rectangular thin sections were cut into 25 millimeter diameter round thin sections, to fit the SIMS sample holders. The round thin sections were cleaned and gold coated (200 Å thick). For sulfur isotope analysis, a 1.8 nA primary beam of Cs^- was accelerated (+10 kV) onto the sample surface with a sputtering diameter of 25 μm. The instrument operated at a 200 V sample offset for sulfur, −10 kV secondary accelerating voltage and at mass resolving power of 350. For detailed description of operating conditions see Riciputi et al. (1998). Ions were detected with an ETP electron multiplier coupled with and ion-counting system and an overall dead time of 34 ns. $^{32}S^-$ and $^{34}S^-$ were detected sequentially by switching the magnetic field. A typical analysis lasted 6 min, comprising 50 cycles of analysis.

During the measurement process by SIMS, an intrinsic mass dependent bias is introduced, which is referred to as instrumental mass fractionation (IMF) and typically favors the low mass isotope. The greatest contributor to the IMF is the ionization process, which depends most strongly upon sample characteristics (i.e., chemical composition). This is referred to as compositionally dependent fractionation or "matrix effects" (e.g., Riciputi et al., 1998). Therefore, accurate isotopic SIMS analysis requires that IMF be corrected for by standardizing the IMF using mineral standards that are compositionally similar to the unknown. SIMS results from the standard are compared to its accepted isotopic composition in

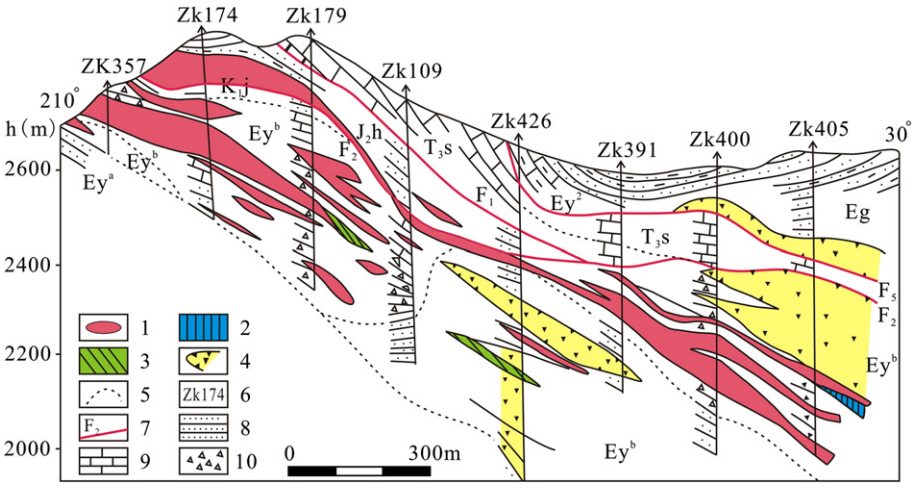

Fig. 3. Geological section of Beichang–Paomaping ore blocks in the Jinding Zn–Pb deposit. 1—Pb–Zn ore. 2—Pyrite ore. 3—Celestite ore. 4—Gypsum ore. 5—Strata boundary. 6—Drilling No. 7—Numbered faults. 8—Siltstone. 9—Limestone. 10—Limestone breccias. Other stratigraphic markers are similar to those in Fig. 2.

order to calculate a correction factor that is applied to the unknowns measured during the same analysis session (e.g. Leshin et al., 1998).

The standards used in this study were large, homogeneous sulfide grains from the Balmat mine, New York (Crowe and Vaughan, 1996). These standards are pyrite with a $\delta^{34}S$ of +15.1‰ (±0.3‰), sphalerite (+14.0‰ ± 0.3‰) and galena (+15.6‰ ± 0.3‰) with the overall spot-to-spot analytical precision of ~0.4‰. Data is reported in the conventional δ-notation relative to the Vienna-Canyon Diablo Troilite (V-CDT) standard. Sulfur isotope analyses consisting of 21 spots on pyrite, 37 spots on galena and 48 spots on sphalerite from diverse mineralization types are summarized in Table 1 with examples in Fig. 6.

4. Results

The results showed a much wider range of $\delta^{34}S$ values from −42.1‰ to 7.7‰, than previously published sulfur isotopic data (−30.4‰ to −1.8‰) produced by bulk analysis (Ye et al., 1992; Zhou and Zhou, 1992). In this paper, we were able to correlate our in situ, micro-analytical, sulfur isotopic data with distinct generations of sulfides and textures (Figs. 7 and 8). Stage 1 sulfides showed the overall $\delta^{34}S$ values ranging from −42.1‰ to −10.2‰ (Fig. 7a). Fine-grained disseminated sulfides hosted in sandstones showed a wide $\delta^{34}S$ range from −42.1‰ to −10.4‰, whereas massive sulfides hosted in limestone breccias had a narrow range of $\delta^{34}S$ values from −28.6‰ to −10.2‰. Sulfides of stage 2 had higher $\delta^{34}S$ values from −8.4‰ to 7.7‰ (Fig. 7b).

Fig. 8 showed the variation in $\delta^{34}S$ values for different sulfide minerals from the Jinding Zn–Pb deposit. Stage 1 pyrite had $\delta^{34}S$ values from −26.9‰ to −12.6‰, similar to coeval galena (−39.6‰ to −10.2‰) and sphalerite (−42.1‰ to −10.4‰). Stage 2 galena had $\delta^{34}S$ values from −8.4‰ to 7.7‰, whereas stage 2 sphalerite had $\delta^{34}S$ values from −8.3‰ to 2.9‰. Different ore blocks in the Jinding deposit displayed a wide range of $\delta^{34}S$ values of sulfide minerals, especially in the Beichang and Fengzishan blocks. Some extremely negative $\delta^{34}S$ values (<−30‰) were found in the stage 1 sulfides from the Fengzishan block, which had been less reported for the Jinding deposit.

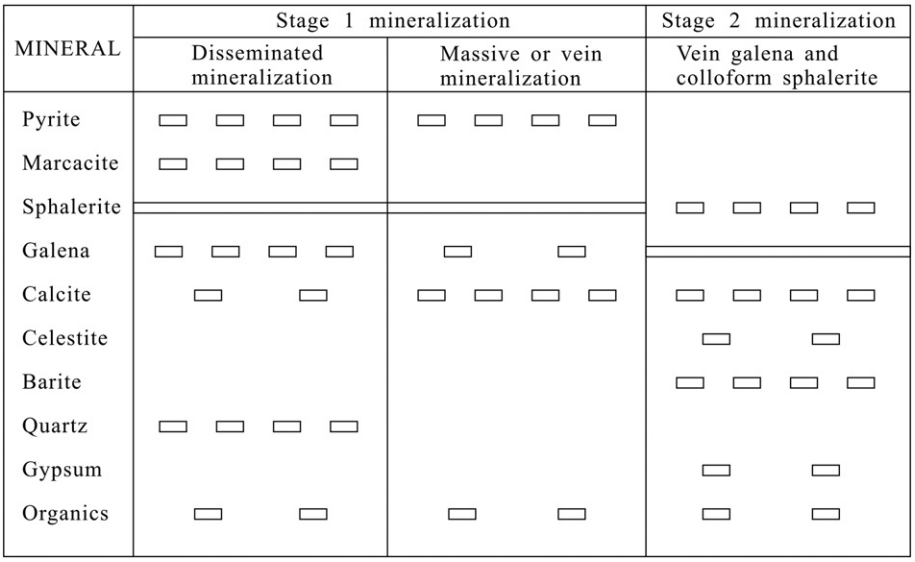

Fig. 4. Simplified paragenetic sequence of major sulfides and gangue minerals from the Jinding Zn–Pb deposit. Stages are defined primarily by sulfide associations and textural variations at the thin section scale. Solid bars represent the distribution of major minerals within a given stage; four broken bars represent minor occurrences; two broken bars represent trace occurrences.

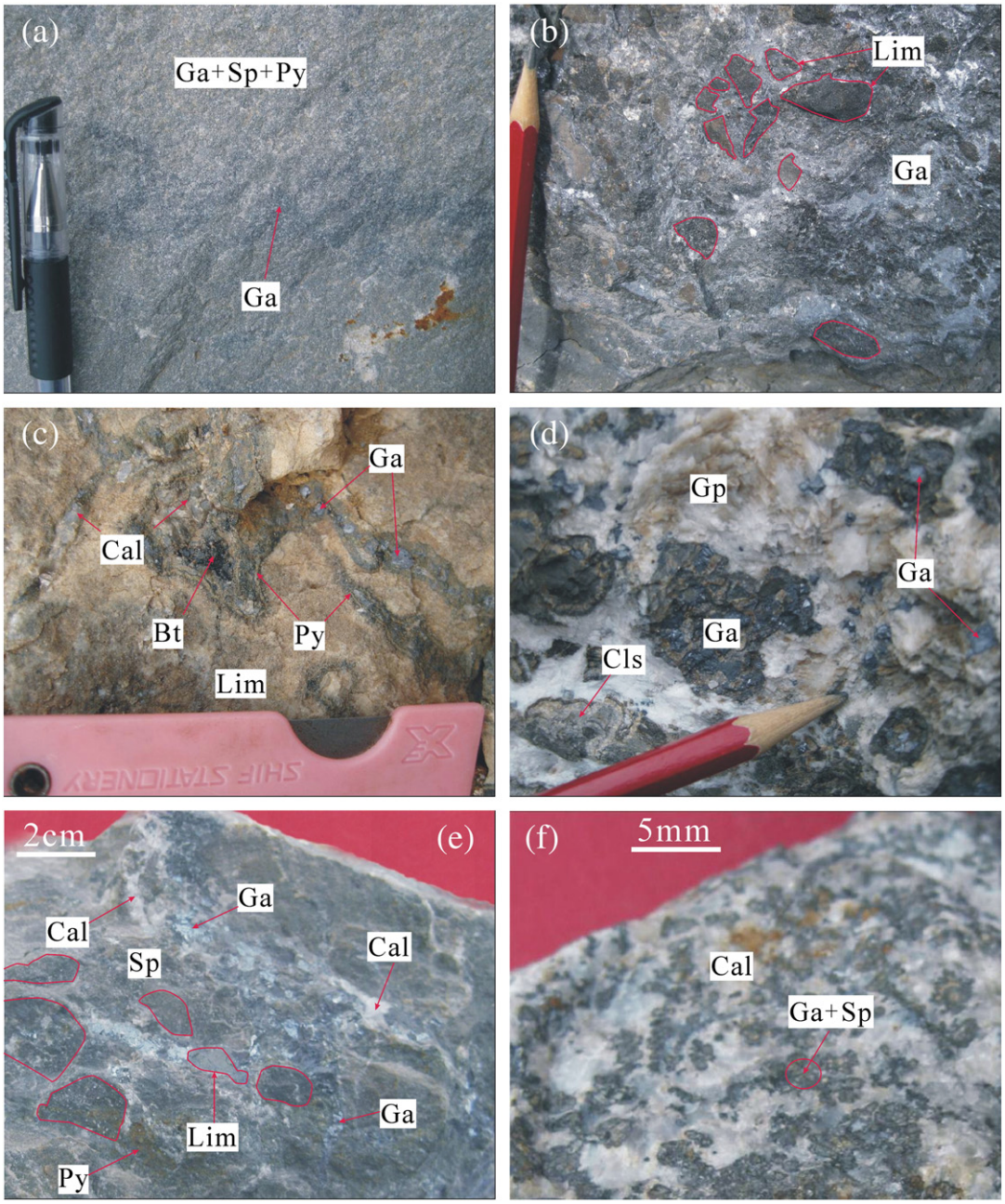

Fig. 5. Mineralization types from the Jinding Zn–Pb deposit. (a) Disseminated sulfides of stage 1 in sandstone are crosscut by the galena vein of stage 2. (b) Massive galena of stage 2 cements limestone breccias. (c) Sulfide vein consisting of galena and pyrite of stage 2 fills in the fractures between breccias, and is intergrown with organics (bitumen) and calcite. (d) Coarse-grained galena of stage 2 is intergrown with celestite and gypsum. (e) Coarse-grained galena vein of stage 2 crosscuts massive sphalerite of stage 1 in limestone breccias. (f) Limestone-hosted ore shows colloform sphalerite and galena of stage 2. Abbreviations: Bt—bitumen, Cal—calcite, Cls—celestite, Ga—galena, Gp—gypsum, Lim—limestone breccias, Py—pyrite, Sp—sphalerite.

5. Discussions

The sulfur isotopes ($\delta^{34}S$) of ore deposits are generally able to place important constraints on the nature of the ore-forming fluid, and the genetic processes for mineralization (e.g., sources of reduced sulfur, mechanisms for sulfate reduction, and related physico-chemical conditions) (Jørgensen, 1979; Ohmoto and Rye, 1979; Ohmoto, 1992; Basuki et al., 2008; Wagner et al., 2010). The most striking characteristics of sulfur isotopes from the Jinding Zn–Pb deposit are the highly variable and low $\delta^{34}S$ values for stage 1 sulfide minerals and the relatively higher $\delta^{34}S$ values for stage 2 sulfide minerals (Figs. 7 and 8).

5.1. Source(s) of sulfur and sulfate reduction mechanisms

Numerous studies (Sakai, 1968; Ohmoto, 1972; Peevler et al., 2003; Ferrini et al., 2010) have shown that there are several factors that could affect the sulfur isotopic composition of sulfide minerals. These factors include temperature, pH and f_{O_2} of the fluid, as well as the $\delta^{34}S$ value of the H_2S responsible for precipitating sulfide minerals. Because sulfur isotopic fractionation between the reduced sulfur species in solution such as H_2S and sulfide minerals (like FeS_2, ZnS and PbS) at low temperatures (<350 °C) is very small (Peevler et al., 2003), the large range in $\delta^{34}S$ values of sulfides from the Jinding deposit is impossible to be

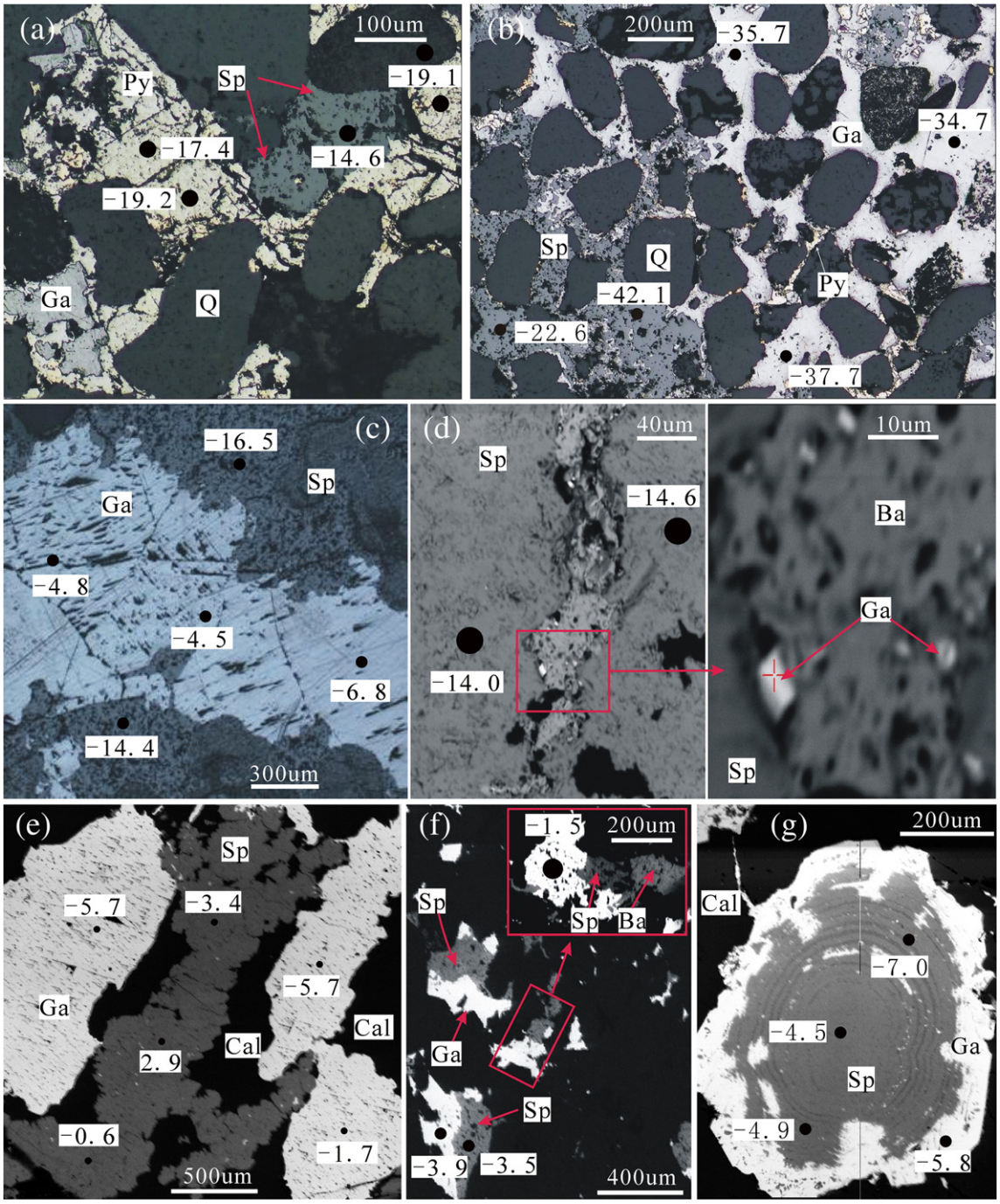

Fig. 6. Photomicrographs in reflected light and back-scattered electron images showing representative textures of mineral associations of different mineralization stages and $\delta^{34}S_{V\text{-}CDT}$ values of sulfide minerals. (a) Galena, sphalerite and pyrite of stage 1 occur interstitial to quartz in sandstone. (b) Stage 1 sulfide cements in sandstones. (c) Coarse-grained galena vein of stage 2 crosscuts the massive sphalerite of stage 1 in limestone breccias. (d) The vein of stage 2 is composed of barite and galena (inset), which crosscuts the massive sphalerite of stage 1 in limestone breccias. (e) Coarse-grained sphalerite and galena of stage 2 in sandstones. (f) Galena-dominated sulfide vein of stage 2 consists of sphalerite and barite (inset) in sandstones. (g) Colloform sphalerite of stage 2 shows zonal textures intergrown with galena in limestone breccias. Abbreviations: Ba—barite, Cal—calcite, Ga—galena, Py—pyrite, Q—quartz, Sp—sphalerite.

caused by changes in fluid temperature. In addition, within the stability field of pyrite, not even significant changes in pH and f_{O_2} would produce the large range in $\delta^{34}S$ values observed (Ohmoto, 1972). Therefore, the large range in $\delta^{34}S$ values from the Jinding deposit is likely caused by changes in the $\delta^{34}S$ value of H_2S in solution when sulfide minerals precipitated.

Several potential sulfur sources may possibly be involved in hydrothermal mineralization, including mantle sulfur ($\sum\delta^{34}S = 0‰$), oceanic sulfate ($\sum\delta^{34}S = \sim 20‰$), and biogenic sulfur with greatly varied negative $\delta^{34}S$ values (Ohmoto and Rye, 1979). In general, we cannot judge the source of sulfur in hydrothermal solution only by the $\delta^{34}S$ values of hydrothermal minerals, but should take full account of the physico-chemical conditions of the ore-forming solutions (Ohmoto, 1972). Given that stage 1 mineral assemblage usually shows pyrite, sphalerite, galena and calcite (Fig. 4) that might form in low f_{O_2} and low pH conditions (Luo et al., 1994), the $\delta^{34}S$ values of sulfides are approximately equal to the $\sum\delta^{34}S$ value of the ore-forming fluid. By contrast, stage 1 shows the typical feature of biogenic sulfur that is generally associated with bacterial sulfate reduction (BSR) (Fig. 9). However, barite began to be present in the stage 2 mineral association, indicating that the f_{O_2} became high in the ore-forming fluid. In this case, the $\delta^{34}S$ values of barite are roughly equivalent to the $\sum\delta^{34}S$ value of

Table 1
Short descriptions and sulfur isotopes data ($\delta^{34}S_{V\text{-}CDT}$ ‰) of sulfide minerals.

Sample no.	Location	Spot no.	Mineral	$\delta^{34}S_{V\text{-}CDT}$ (‰)	2σ (‰)
Stage 1: disseminated sulfides in sandstone (n = 17)					
①	Beichang	1	Pyrite	−22.3	0.9
		2	Pyrite	−19.3	0.9
		3	Pyrite	−12.6	0.9
		4	Pyrite	−17.1	0.9
		5	Pyrite	−22.4	0.9
		6	Pyrite	−17.4	0.9
		7	Pyrite	−19.2	0.7
		8	Pyrite	−19.1	0.7
		1	Sphalerite	−10.4	0.7
		2	Sphalerite	−17.5	0.7
		3	Sphalerite	−19.3	0.7
		4	Sphalerite	−14.4	0.7
		5	Sphalerite	−14.6	0.7
		1	Galena	−15.5	0.8
		2	Galena	−10.5	0.8
		3	Galena	−15.0	0.8
		4	Galena	−12.0	0.8
Stage 1: disseminated sulfides in sandstone (n = 17)					
②	Fengzishan	1	Pyrite	−26.9	0.6
		2	Pyrite	−24.4	0.7
		3	Pyrite	−26.2	0.7
		4	Pyrite	−26.0	0.7
		5	Pyrite	−25.3	0.7
		6	Pyrite	−24.9	0.7
		1	Sphalerite	−40.3	0.7
		2	Sphalerite	−34.4	0.7
		3	Sphalerite	−42.1	0.7
		4	Sphalerite	−22.6	0.7
		5	Sphalerite	−34.9	0.7
		1	Galena	−34.7	0.8
		2	Galena	−36.1	0.8
		3	Galena	−35.7	0.8
		4	Galena	−29.2	0.8
		5	Galena	−39.6	0.8
		6	Galena	−37.7	0.8
Stage 1: massive sulfides in sandstone (n = 6)					
③	Jiayashan	1	Sphalerite	−20.3	0.7
		2	Sphalerite	−27.5	0.7
		3	Sphalerite	−20.7	0.7
		1	Galena	−28.6	0.8
		2	Galena	−23.7	0.8
		3	Galena	−11.4	0.8
Stage 1: massive sulfides in sandstone (n = 2)					
④	Beichang	1	Sphalerite	−16.0	0.7
		2	Sphalerite	−11.0	0.7
Stage 1: massive sulfides in limestone breccia (n = 5)					
⑤	Paomaping	1	Sphalerite	−12.3	0.7
		2	Sphalerite	−14.0	0.7
		3	Sphalerite	−14.1	0.7
		4	Sphalerite	−13.7	0.7
		5	Sphalerite	−14.6	0.7
Stage 1: massive sulfides in limestone breccia (n = 2)					
⑥	Paomaping	1	Galena	−23.1	1.2
		2	Galena	−21.3	1.2
Stage 1: massive sulfides in limestone breccia (n = 4)					
⑦	Beichang	1	Sphalerite	−16.5	0.7
		2	Sphalerite	−14.4	0.7
		3	Sphalerite	−16.5	0.7
		4	Sphalerite	−23.5	0.7
Stage 1: massive sulfides in limestone breccia (n = 2)					
⑦	Beichang	1	Pyrite	−18.0	0.7
		2	Pyrite	−16.3	0.6
Stage 1: sulfide vein in limestone breccia (n = 14)					
⑧	Beichang	1	Galena	−14.7	0.8
		2	Galena	−18.8	0.8
		3	Galena	−25.2	0.8
		4	Galena	−12.7	0.8
		5	Galena	−10.2	0.8
		1	Sphalerite	−13.2	0.9
		2	Sphalerite	−23.8	0.9
		3	Sphalerite	−13.2	0.9
		4	Sphalerite	−16.9	0.9
		1	Pyrite	−14.9	0.7
		2	Pyrite	−17.3	0.7
		3	Pyrite	−12.7	0.7
		4	Pyrite	−15.5	0.7
		5	Pyrite	−13.2	0.7
Stage 2: sulfide vein in sandstone (n = 10)					
⑨	Fengzishan	1	Sphalerite	−6.0	0.6
		2	Sphalerite	−4.1	0.6
		3	Sphalerite	−3.5	0.6
		4	Sphalerite	−5.5	0.6
		5	Sphalerite	−5.2	0.6
		1	Galena	−7.2	0.8
		2	Galena	−7.2	0.8
		3	Galena	−3.9	0.8
		4	Galena	−6.7	0.8
		5	Galena	−1.5	0.8
Stage 2:sulfide vein in sandstone (n = 6)					
④	Beichang	1	Sphalerite	−3.4	0.7
		2	Sphalerite	2.9	0.7
		3	Sphalerite	−0.6	0.7
		1	Galena	−1.7	0.8
		2	Galena	−5.7	0.8
		3	Galena	−5.9	0.8
Stage 2: galena vein in limestone breccia (n = 2)					
⑦	Paomaping	1	Galena	−6.9	1.2
		2	Galena	−8.4	1.2
Stage 2: galena vein in limestone breccia (n = 4)					
⑧	Beichang	1	Galena	−6.8	1.2
		2	Galena	−4.5	1.2
		3	Galena	−4.8	1.2
		4	Galena	−7.2	1.2
Stage 2:colloform sulfides in limestone breccia (n = 15)					
⑩	Beichang	1	Sphalerite	−7.3	0.9
		2	Sphalerite	−8.3	0.9
		3	Sphalerite	−7.3	0.9
		4	Sphalerite	−5.7	0.9
		5	Sphalerite	−5.8	0.9
		6	Sphalerite	−6.8	0.9
		7	Sphalerite	−6.7	0.9
		8	Sphalerite	−6.9	0.9
		9	Sphalerite	−5.7	0.9
		10	Sphalerite	−4.9	0.9
		11	Sphalerite	−4.5	0.9
		12	Sphalerite	−7.0	0.9
		1	Galena	−8.3	0.8
		2	Galena	−5.8	0.8
		3	Galena	7.7	0.8

the ore-forming fluid, far more than $\delta^{34}S$ values of sulfides. Luo et al. (1994) reported the $\delta^{34}S$ values of barite associated with stage 2 mineralization were in the range from 11.2‰ to 16.3‰, similar to those (10.8‰–15.7‰) of evaporites in the Lanping basin (Zhang and Wen, 2012). Therefore, these evaporitic rocks likely acted as the source of sulfur for stage 2 mineralization, and the reduced sulfur (H_2S) was produced by means of sulfate reduction.

Stage 1 sulfides show the most varied and negative $\delta^{34}S$ values, suggesting that H_2S was derived from BSR mechanism. The BSR mechanism is the most efficient means for causing a large fractionation between SO_4^{2-} and H_2S at low temperatures (Chen et al., 1994; Habicht et al., 1998). The sulfur isotope fractionation between SO_4^{2-} and H_2S caused by BSR is reported to be between 4‰ and 46‰, with an average of 21‰ (Canfield and Teske, 1996; Habicht et al., 1998). Moreover, an extreme fractionation (~46‰) would be obtained only if at a slow rate during BSR process (Rees, 1973). Due to irreversibility, the BSR reaction usually brings about large sulfur isotopic fractionation with biogenic sulfur circulating in nature (Chen et al., 1994). This process generally causes a fractionation of less than 46‰ (Chang et al., 2007). However, part of $\delta^{34}S$ data of sulfides (−42.1‰ to −30‰) from the Jinding deposit show larger fractionations from evaporites, similar to those of sulfides in modern oceanic sediments or euxinic waters

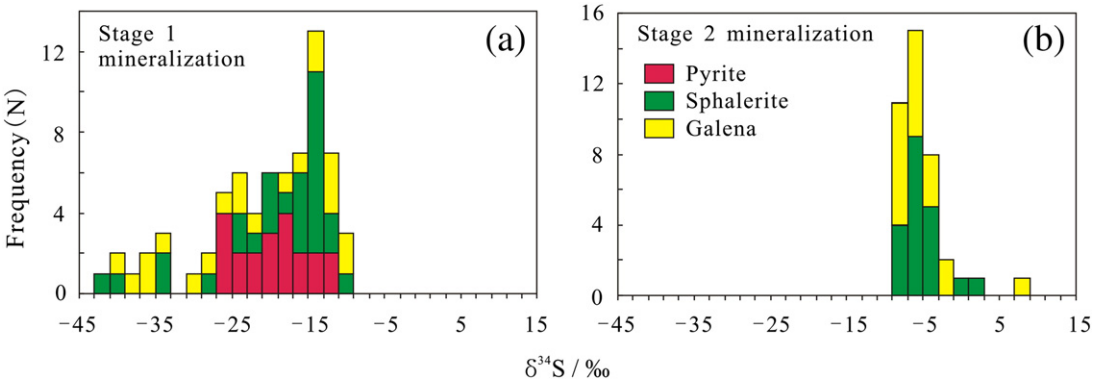

Fig. 7. Histograms displaying sulfur isotopic compositions of sulfide minerals from different mineralization stages.

which are considered as a result of bacterial sulfate reduction combined with disproportionation of intermediate sulfur species (like S^0, $S^2O_3^{2-}$ and SO_3^{2-}) (Canfield and Thamdrup, 1994; Canfield and Teske, 1996; Habicht et al., 1998). In general, the process of bacteria involved disproportionation can cause a fractionation, up to 7‰ to 11‰, within both lacustrine and marine sulfur cycle, which leads to an enrichment of ^{32}S in sediments (Canfield and Thamdrup, 1994; Canfield and Teske, 1996; Cypionka et al., 1998; Habicht et al., 1998). When the pre-existing sulfides associated with bacterial sulfate reduction was oxidized to elemental sulfur (S^0), the S^0 was microbially disproportionated by

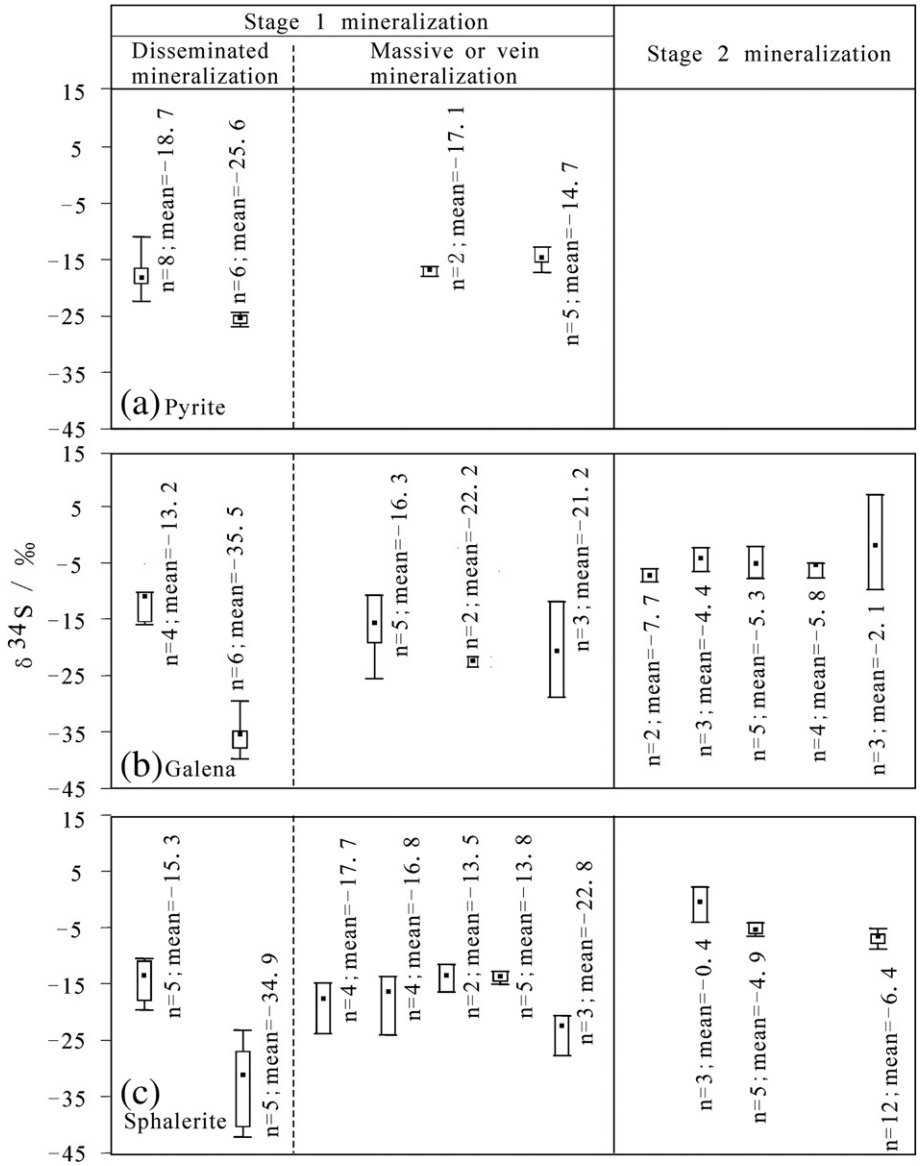

Fig. 8. Box plots showing variations in sulfur isotopic composition of sulfide minerals from stage 1 and 2 mineralization. Number of analyses for each stage or type, and mean value are indicated next to each box plot. The line represents the range of sulfur isotopes, vertical bar is 25% to 75% range, and the filled square is the mean value.

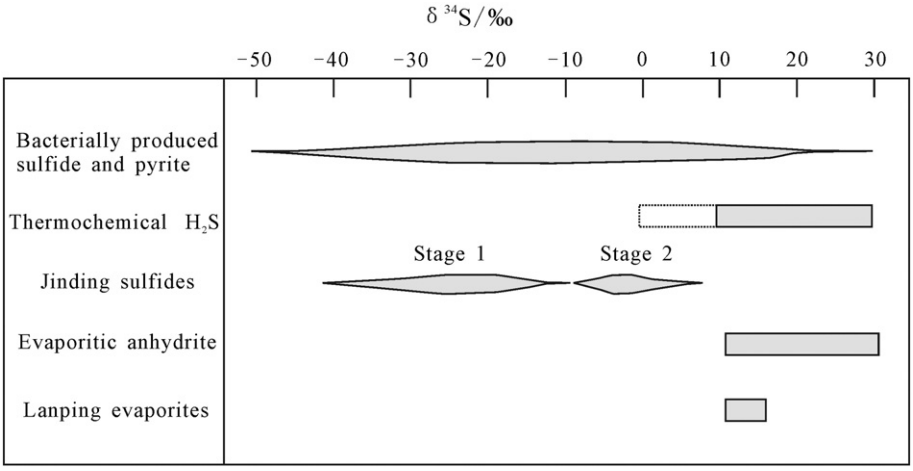

Fig. 9. Sulfur isotopic compositions of sulfides from the Jinding deposit, comparing with the typical ranges for naturally occurring sulfur isotopes from BSR and TSR mechanisms. Modified after Warren (1999).

the chemolithotrophic bacterial metabolism to sulfate and sulfide, as follows: $4S^0 + 4H_2O \rightarrow SO_4^{2-} + 3H_2O + 2H^+$, accompanied by relatively large sulfur isotopic fractionation (Thamdrup et al., 1993). So the cycle repeated, it would produce more ^{34}S-depleted sulfides than was formed directly by bacterial sulfate reduction (Chang et al., 2007). This mechanism could be used to interpret the extremely ^{34}S-depleted sulfides in stage 1 from the Jinding deposit. However, BSR characteristically occurs at temperatures of less than 60 °C to 80 °C (Machel and Foght, 2000; Machel, 2001), although occasionally it has been found to occur up to 110 °C at some modern hydrothermal vents (Jørgensen et al., 1992). These temperatures are far lower than the mineralizing temperatures of 115–234 °C from fluid inclusions in stage 1 sphalerite (Zeng, 2007). Therefore, BSR could have happened in non-mineralizing sites or before mineralization (Leach et al., 2005). Then, reduced sulfur could be transported from the primary origin to the Jinding dome where it formed a reducing gas cap, which could rapidly precipitate sulfides when it mixed with a metal-bearing fluid.

The feature of the $\delta^{34}S$ values of stage 2 sulfides indicates that H_2S might be derived either from bacterial sulfate reduction (BSR), or thermochemical sulfate reduction (TSR), or both, comparing with the typical ranges for naturally occurring sulfur isotopes under BSR and TSR mechanisms (Fig. 9). If the system remains closed to SO_4^{2-} but open to H_2S (i.e., sulfate reduction proceeds at a faster rate than sulfate supply, but open to H_2S in the sense that H_2S is fixed instantaneously as sulfide minerals, or removed), precipitation of ^{32}S-enriched sulfides would drive the composition of the remaining sulfate to higher (^{34}S-enriched) values. During the initial stages of sulfide, BSR process could have produced highly fractionated sulfur and sulfides with very low $\delta^{34}S$ values ($< -20‰$). As the system evolved, the sulfur reservoir became closed to SO_4^{2-} but open to H_2S. Under this condition the $\delta^{34}S$ (H_2S) would increase with increasing degree of sulfate reduction. Consequently, the $\delta^{34}S$ of the accumulated sulfides would also increase with increasing degree of sulfate reduction. Thus, Rayleigh fractionation of sulfur isotope can explain the increasing $\delta^{34}S$ values of stage 2 sulfides. However, the relationship of mineral cutting suggests two separate mineralizing events for stage 1 and stage 2. The intra-crystalline variation of $\delta^{34}S$ values is usually very small, inconsistent with that of BSR process in a closed system (Peevler et al., 2003; Drake et al., 2013). Even though the BSR process for stage 1 could last to the stage 2, from the point of view of mass conservation some sulfur-bearing compounds with extraordinary ^{34}S enrichment should be found in the Jinding deposit, but it wasn't. In addition, some sulfate minerals (like barite, celestite and anhydrite) precipitated temporally with stage 2 sulfides, which argued that it wasn't possible to keep the system closed to SO_4^{2-} during the stage 2 period. Consequently, the BSR mechanism in the system closed to SO_4^{2-} but open to H_2S will be excluded as the means of H_2S production in stage 2.

Alternatively, the $\delta^{34}S$ variations of stage 2 sulfides could also be interpreted by thermochemical sulfate reduction (TSR) that may cause a fractionation of ~0 to 20‰ (Kiyosu and Krouse, 1990; Machel et al., 1995) at relatively higher temperatures (>80 °C to 100 °C, Orr, 1974; Machel et al., 1995; Machel, 2001). The possibility of TSR reaction occurring at the Jinding deposit could be assessed by considering the following aspects: (1) thermal regime of 80 °C or higher caused by geothermal gradation, or heated by hot mineralizing fluid over long time (Luo et al., 1994; Wen et al., 1995); (2) sufficient SO_4^{2-} anions provided by dissolution of evaporites in the Lanping basin (Xue et al., 2007a; He et al., 2009); and (3) reductants such as solid organic bitumen, petroleum sulfur or methane from the fossil-oil reservoir (Chang and Zhang, 2003; Guo et al., 2003; Fu et al., 2005; Xue et al., 2007b, 2009; Gao et al., 2012). Because multiple evaporitic horizons of the different epochs recognized in the Lanping basin could provide SO_4^{2-} to the hydrothermal system, the $\delta^{34}S$ values of sulfates dissolved in the fluid were in a relatively large range from 10.8‰ to 15.7‰ (Zhang and Wen, 2012). In view of sulfur isotopic fractionation ($\Delta\delta^{34}S_{SO_4^{-}H2S} < 20‰$) caused by TSR process, the resulted $\delta^{34}S$ values of sulfides will locate within the range from −9.2‰ to 4.3‰, approximately overlapping with those (−8.4‰–7.7‰) of stage 2 sulfides from the Jinding deposit.

5.2. Mechanism of mineralization of the Jinding deposit

Three general models have been proposed to account for the transport and deposition of base metal sulfides, namely mixing model, sulfate reduction model and reduced sulfur model, in the sediment-hosted base metal deposits (Sverjensky, 1981; Anderson and MacQueen, 1982). The mixing model implies the coexistence of two fluids, one of which is the ore-forming fluid containing dissolved metals (usually thought of as chloride complexes of zinc and lead), but the other could be an H_2S-containing fluid of which H_2S is mainly derived from bacterial sulfate reduction. The two fluids transport to the site of the deposition and mix that leads to sulfide precipitation (Anderson, 1973; Beales, 1975; Anderson, 1983, 1991, 2008). The mixing model is especially applied to the MVT deposits where abundant evaporites develop. Because acid is produced during sulfide precipitation due to fluid mixing ($H_2S_{aq} + Zn^{2+} \rightarrow ZnS_s + 2H^+$, Merce et al., 2004), the mixing model can interpret widespread presence of carbonatization and dissolution collapse breccias (Anderson, 1983). The Jinding Zn–Pb deposit is macro-morphologically divided into the upper stratiform or tabular sandstone-type ores, and the lower lentoid or tubular limestone breccia-type ores. Similar distribution of ore bodies in the MVT deposits has been described and interpreted as a result of a

reduced gas phase control (Anderson, 2008). From the point of view of sulfur isotopic fractionation, such greatly varied negative $\delta^{34}S$ values of stage 1 sulfides could solely be associated with bacterial sulfate reduction. The pre-existing bacteriogenic sulfur might be transported to form a reduced gas cap in the Jinding dome. H_2S provided by the gas cap in the presence of available metals would result in rapid precipitation of sulfide minerals with a very fine-grained texture, as is a common texture of stage 1 sulfides in the Jinding deposit.

Sulfate reduction model means base metals and oxidized sulfur (SO_4^{2-}) are transported by the same fluid to the site of deposition where the oxidized sulfur is reduced to H_2S by organic matter causing the precipitation of sulfides (Olson, 1984; Garven, 1985). Given the presence of a great amount of barite and celestite in the stage 2 mineralization, it is inferred that the content of SO_4^{2-} in the fluid should be high. Luo et al. (1994) studied the H–O isotopes of late celestite and considered the ore-forming fluid had shifted to meteoric water in the stage 2 mineralization. During the infiltration process of the meteoric water, the fluid reacted with the evaporitic rocks and dissolved sulfates. Then, it leached metals from the wall rocks and transported them as sulfate- or sulfite-complexes to the Jinding dome where the oxidized sulfur was reduced to H_2S by organic matters. Usually, various kinds of organic matter, such as kerogen, light oil, hydrocarbon gases, heavy oil, bitumen with different occurrences and maturation, and oil-and-methane-inclusions in calcite and celetitite have been observed, which suggest ever an ancient oil–gas reservoir in the Jinding dome (Xue et al., 2006, 2009). If methane was provided, reaction with sulfate in ore solution would be slow, resulting in precipitation of well-formed crystals as metals were present (Anderson, 2008). This mechanism might account for coarse-grained occurrence of galena in stage 2.

Base metals and reduced sulfur are transported in the same fluid at low pH, and precipitation is caused by an increase in pH, cooling, or a reduction in salinity due to dilution, which is referred to as the reduced sulfur model (Helgeson, 1969; Anderson, 1973; Sverjensky, 1981). Under the condition of <200 °C, it is extremely difficult for H_2S to coexist with metals in the oilfield water. The reduced sulfur model is generally applied to the deposits that have neither evaporites nor traces of sulfate reduction. In any case, the mechanism seems improbable for the Jinding deposit, where the ore-forming fluid would have to maintain a low pH, even if traveling through terrestrial alkaline red clastic rocks.

The Jinding deposit was considered to be formed at 33 to 28 Ma (Wang et al., 2009), temporally corresponding to the late-collisional transition stage of India–Asian continental collision that meant the stress regime in Sanjiang region shifted from collisional compression to strike-slip (Hou and Cook, 2009). At that time, crustal compression and shortening in the Lanping area reached a climax and started to relax. Under this tectonic setting, mantle-derived magmas emplaced upward and formed alkali intrusions which might provide the heat energy to drive the hydrothermal system (Wang et al., 2009). Some geophysical and geological progresses suggested igneous intrusions might hide underneath the Jinding deposit (Ge et al., 1999; Zhang et al., 2000). Therefore, we can approximately conclude the hydrothermal mineralizing process of the Jinding deposit. Because of continued India–Asian collision, the surrounding orogenic belt lifted relative to the Paleogene foreland basins in the eastern and northern margins of the Tibetan plateau, and strong compression resulted in the thrusting of these basins. In the Lanping basin, the fluid generated from the orogen migrated laterally along gently-dipping detachment faults of the thrust systems toward the basin and evolved into metal-bearing fluid through interaction with country rocks. The metal-bearing fluid migrated vertically along major thrust faults (F_2) and finally deposited sulfide minerals when it came across the H_2S-rich fluid, of which H_2S was derived from BSR for stage 1 mineralization in the open spaces induced by thrust–nappe structures at shallow levels. During the stage 2 mineralization, the meteoric water infiltrated and reacted with evaporitic rocks, and then it leached metals and transported them as sulfate- or sulfite-complexes to the Jinding dome where the oxidized sulfur was reduced by organic matters to H_2S, leading to sulfide precipitation.

5.3. Comparison with other sulfide deposits in the Lanping basin

The sulfur isotopic compositions of sulfides from the Jinding Zn–Pb deposit are compared with $\delta^{34}S$ values of other sulfide deposits (Jinman Cu ore belt, Baiyangping Ag–Cu–Pb–Zn ore belt and Sanshan Pb–Zn ore belt) in the Lanping basin (Fig. 10). The $\delta^{34}S$ values of sulfides from the Jinman Cu ore belt vary from −23‰ to 12‰, with the peak ranging

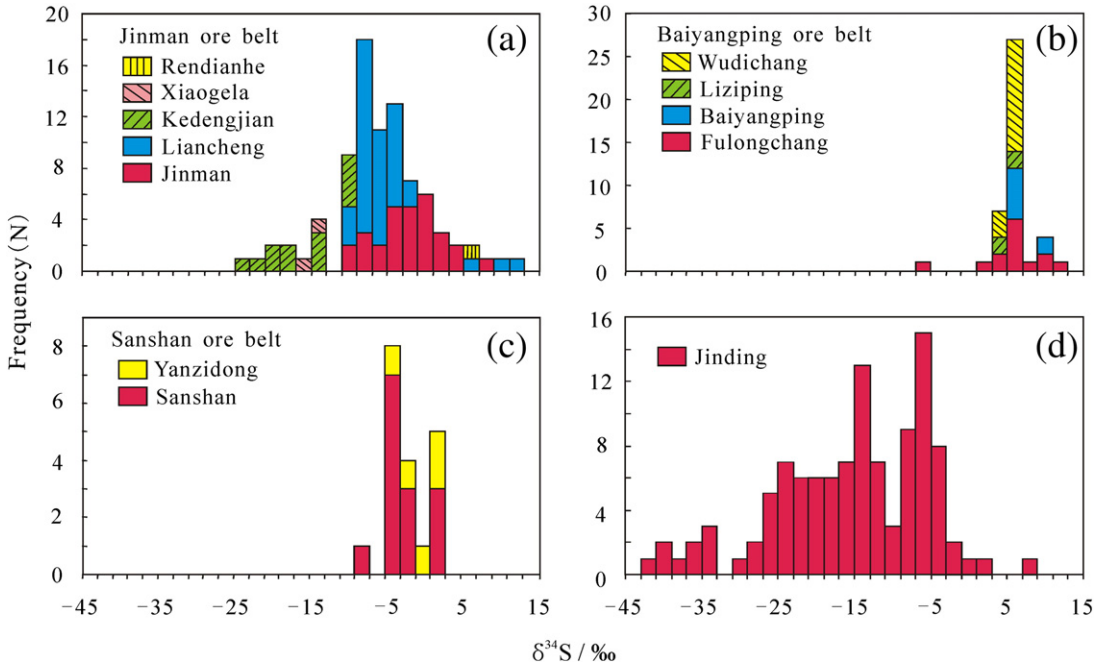

Fig. 10. Histograms showing the sulfur isotopic composition of sulfide minerals from several deposits in the Lanping basin. Sulfur isotopic data of the deposits, except Jinding, were measured by the conventional analytical method.

from −8‰ to −2‰ (Ji and Li, 1998; Li, 2002; Zhao, 2006; Zhang and Wen, 2012; and reference therein). Baiyangping ore belt has $\delta^{34}S$ values that range from +3‰ to +7‰ (Wei, 2001; Wang and He, 2003; Li et al., 2005; Wang et al., 2011). Sanshan ore belt displays $\delta^{34}S$ values varying from −7.3‰ to 2.1‰ with the peak ranging from −5‰ to +1‰ (M.Q. He et al., 2004; Zhao, 2006). Previous studies proposed that the sulfur was mainly derived from a mantle source, not excluding the contribution of biogenic sulfur to individual deposit (Ji and Li, 1998; Li, 2002; M.Q. He et al., 2004; Zhao, 2006). However, this view was also questioned by some researchers who suggested the sulfur might be resulted from sulfate reduction (Wang et al., 2011; Zhang and Wen, 2012). By contrast, the Jinding deposit shows the absolutely dominant numbers of greatly varied negative $\delta^{34}S$ values of sulfide minerals. The overall lower $\delta^{34}S$ values of sulfides distinguish the Jinding deposit from other sulfide deposits located in the Lanping basin, which indicates that biogenic sulfur might have played a key role in the mineralization of the Jinding Zn–Pb deposit.

6. Conclusions

We have used the secondary ion mass spectrometry (SIMS) to determine the sulfur isotopic compositions of sulfide minerals from different mineralization stages in the Jinding Zn–Pb deposit. In situ sulfur isotopic analyses of sulfide minerals show the widest range and lowest $\delta^{34}S$ values (−42.1‰ to −30‰) ever reported for the Jinding deposit. Stage 1 has $\delta^{34}S$ values from −42.1‰ to −10.2‰ with the majority ranging from −26‰ to −14‰, suggesting a biogenic sulfur source associated with bacterial sulfate reduction. Stage 2 has higher $\delta^{34}S$ values between −8.3‰ and 7.7‰ that indicates reduced sulfur was likely produced by thermochemical sulfate reduction. By contrast, biogenic sulfur might have played a key role in the mineralization process, especially during the early stage of formation of the Jinding Zn–Pb deposit.

The most reasonable scenario for the stage 1 mineralization is a metal-bearing brine mixing with an H_2S-rich fluid, thereby causing rapid sulfide precipitation. Till the stage 2, the ore-forming fluid shifted to the meteoric water that infiltrated and reacted with evaporitic rocks, leached metals and transported them as sulfate- or sulfite-complexes to the Jinding dome where the oxidized sulfur was reduced by organic matters to H_2S, leading to precipitation of metal sulfides.

Acknowledgments

The research was supported by the National Basic Research Program (No. 2009CB421005), a NSERC Discovery grant to Fayek and the CRC program, the strategy surveys program of the tri-Rare metal resources of China (No. 12120113078200), and the 12th Five-Year Plan Project of State Key Laboratory of Ore-deposit Geochemistry, Chinese Academy of Sciences (SKLODG-ZY125-03). We thank Dr. Ravinder Sidhu (Canada) for her assistance in SEM analysis and Breana Hashman for her help with SIMS analysis. Further thanks are due to Dr. Feiyue Wang and Ph.D student Jincheng Luo for their help during the SIMS analysis in Canada.

References

Anderson, G.M., 1973. The hydrothermal transport and deposition of galena and sphalerite near 100 °C. Economic Geology 68, 480–492.
Anderson, G.M., 1983. Some geochemical aspects of sulfide precipitation in carbonate rocks. In: Kisvarsanyi, G., Sheldon, G., Pratt, W., Koenig, J. (Eds.), International Conference on Mississippi Valley-type Lead–Zinc Deposits; Proceedings Volume. University of Missouri-Rolla, Rolla, MO, pp. 61–76.
Anderson, G.M., 1991. Organic maturation and ore precipitation in Southeast Missouri. Economic Geology 86, 909–926.
Anderson, G.M., 2008. The mixing hypothesis and the origin of Mississippi Valley-type ore deposits. Economic Geology 103, 1683–1690.
Anderson, G.M., MacQueen, R.W., 1982. Ore deposit models-6. Mississippi Valley-type lead–zinc deposits. Geoscience Canada 9, 108–117.
Bai, J.F., Wang, C.H., Na, R.X., 1985. Geological characteristics of the Jinding lead–zinc deposit in Yunnan with a special discussion on its genesis. Mineral Deposits 4, 1–9 (in Chinese with English abstract).
Basuki, N.I., Spooner, 2004. A review of fluid inclusion temperatures and salinities in Mississippi Valley-type Pb–Zn deposits: identifying thresholds for metal transport. Exploration and Mining Geology 11, 1–17.
Basuki, N.I., Taylor, B.E., Spooner, E.T.C., 2008. Sulfur isotope evidence for thermochemical reduction of dissolved sulfate in Mississippi Valley-type zinc–lead mineralization, Bongara area, northern Peru. Economic Geology 103, 783–799.
Beales, F.W., 1975. Precipitation mechanisms for Mississippi Valley-type ore deposits. Economic Geology 7, 943–948.
Bjorlykke, A., Sangster, D.F., 1981. An overview of sandstone lead deposits and their relation to red-bed copper and carbonated hosted lead–zinc deposits. Economic Geology 76, 179–213.
Bradley, D.C., Leach, D.L., 2003. Tectonic controls of Mississippi Valley-type lead–zinc mineralization in orogenic forelands. Mineralium Deposita 38, 652–667.
Canfield, D.E., Teske, A., 1996. Late proterozoic rise in atmospheric oxygen concentration inferred from phylogenetic and sulphur-isotope studies. Nature 382, 127–132.
Canfield, D.E., Thamdrup, B., 1994. The production of ^{34}S-depleted sulfide during bacterial disproportiontion of elemental sulfur. Science 266, 1973–1975.
Chang, X.C., Zhang, J.L., 2003. Geochemical characteristics of oil in the Jinding lead–zinc lease and its implication. Special Oil and Gas Reservoirs 10, 15–19 (in Chinese with English abstract).
Chang, H.J., Chu, X.L., Huang, J., Feng, L.J., Zhang, Q.R., 2007. Sulfur isotope fractionation accompanying bacterial action under sedimentary condition. Geological Review 53, 807–813 (in Chinese with English abstract).
Chen, D.G., Zhi, X.C., Yang, H.T., 1994. Geochemistry. Publishing House of University of science and technology of China, Hefei 301–304 (in Chinese).
Chen, J.Y., Yang, Y.C., Huo, X.G., Shang, R.J., 1995. Tectonic history of Qingling–Qilianshan–Kunlunshan mountains and the matching of both south and north Chinese plates. Geology of Shanxi 13, 1–11 (in Chinese with English abstract).
Chen, K.X., He, L.Q., Yang, Z.Q., Wei, J.Q., Yang, A.P., 2000. Oxygen and carbon isotope geochemistry in Sanshan–Baiyangping copper–silver polymetallogenic enrichment district, Lanping, Yunnan. Geology and Mineral Resources of South China 4, 1–8 (in Chinese with English abstract).
Chi, G.X., Xue, C.J., Lai, J.Q., Qing, H.R., 2007. Sand injection and liquefaction structures in the jinding Zn–Pb deposit Yunnan, China: indicators of an overpressured fluid system and implications for mineralization. Economic Geology 102, 739–743.
Clendenin, C.W., Duane, M.J., 1990. Focused fluid flow and Ozark Mississippi Valley-type deposit. Geology 18, 116–119.
Crowe, D.E., Vaughan, R.G., 1996. Characterization and use of isotopically homogeneous standards for in situ laser microprobe analysis of $^{34}S/^{32}S$ ratios. American Mineralogist 81, 187–193.
Cypionka, H., Smock, A., Böttcher, M.E., 1998. A combined pathway of sulfur compound disproportionation in *Desulfovibrio desulfuricans*. FEMS Microbiology Letters 166, 181–186.
Deloule, E., Allegre, C., Doe, B., 1986. Lead and sulfur isotope microstratigraphy in galena crystals from Mississippi Valley type deposits. Economic Geology 81, 1307–1321.
Deng, J., Hou, Z.Q., Mo, X.X., Yang, L.Q., Wang, Q.F., Wang, C.M., 2010. Superimposed orogenesis and metallogenesis in Sanjiang Tethys. Mineral Deposits 29, 37–42 (in Chinese with English abstract).
Deng, J., Wang, C.M., Li, G.J., 2012. Style and process of the superimposed mineralization in the Sanjiang Tethys. Acta Petrologica Sinica 28, 1349–1361 (in Chinese with English abstract).
Drake, H., Åström, M.E., Tullborg, E.L., Whitehouse, M., Fallick, A.E., 2013. Variability of sulphur isotope ratios in pyrite and dissolved sulphate in granitoid fractures down to 1 km depth — evidence for widespread activity of sulphur reducing bacteria. Geochimica et Cosmochimica Acta 102, 143–161.
Feng, Q.L., 2002. Stratigraphy of volcanic rocks in the Changning–Menglian belt in southwestern Yunnan, China. Journal of Asian Earth Sciences 20, 657–664.
Feng, C.X., Bi, X.W., Hu, R.Z., Liu, S., Wu, L.Y., Tang, Y.Y., Zou, Z.C., 2011. Study on paragenesis–seperation mechanism and sources of ore-forming element in Baiyangping Cu–Pb–Zn–Ag polymetallic ore deposit, Lanping basin, southwestern China. Acta Petrologica Sinica 27, 2609–2624 (in Chinese with English abstract).
Ferrini, V., Fayek, M., De Vito, C., Mignardi, S., Pignatti, J., 2010. Extreme sulphur isotope fractionation in the deep Cretaceous biosphere. Journal of the Geological Society 167, 1009–1018.
Fu, X.G., 2004. Discussion on biogenic and organic mineralization of the Jinding Zn–Pb deposit. Resources Survey and Environment 25, 184–189 (in Chinese with English abstract).
Fu, X.G., Lin, L., Pang, Y.C., Zhu, L.D., Wang, X.L., 2005. Distribution of anthraxolite and metallogeny of the Jinding lead–zinc deposit. Journal of Jilin University (Earth Science Edition) 35, 581–586 (in Chinese with English abstract).
Gao, G.L., 1989. Review of geological origin about Jinding lead–zinc ore deposit. Earth Science 14, 467–475 (in Chinese with English abstract).
Gao, Z.Q., Zhao, Q.H., Tong, Y.H., 2006. Jinman sedimentation–hydrothermal reformation Cu deposit, Lanping. Yunnan Geology 25, 341–347 (in Chinese with English abstract).
Gao, Y.B., Xue, C.J., Zeng, R., 2008. Forming mechanisms of H_2S in the Jinding Pb–Zn deposit, Lanping Basin, Northwest Yunnan Province. Journal of Earth Sciences and Environment 30, 367–372 (in Chinese with English abstract).
Gao, B.Y., Xue, C.J., Chi, G.X., Li, C., Qu, W.J., Du, A.D., Li, Z.X., Gu, H., 2012. Re–Os dating of bitumen in the giant Jinding Zn–Pb deposit, Yunnan and its geological significance. Acta Petrologica Sinica 28, 1561–1567 (in Chinese with English abstract).
Garven, G., 1985. The role of regional fluid flow in the genesis of the Pine Point deposit, Western Canada sedimentary basin. Economic Geology 80, 307–324.
Ge, L.S., Yang, J.H., Guo, X.D., Zou, Y.L., Chen, S.X., Zhang, X.H., 1999. The hidden EW-structure existing in north-western Yunnan and the evidence. Yunnan Geology 18, 155–167 (in Chinese with English abstract).

Gong, W.J., Tan, K.X., Li, X.M., Gong, G.L., 2000. Geochemical characteristics of fluid and mechanism for ore formation in the Baiyangping copper–silver deposit, Yunnan. Geotectonica et Metallogenia 24, 175–181 (in Chinese with English abstract).
Guo, H.H., Chang, X.C., Zhang, J.L., 2003. Geochemistry of late Triassic oil in the Lanping depression and its implications to organic mineralization. Journal of Chang'an University (Earth Science Edition) 25, 1–5 (in Chinese with English abstract).
Habicht, K., Canfield, D.E., Rethemeier, J., 1998. Sulfur isotope fractionation during bacterial reduction and disproportionation of thiosulfate and sulfite. Geochimica et Cosmochimica Acta 62, 2585–2595.
He, L.Q., Chen, K.X., Yu, F.M., Wei, J.Q., Yang, A.P., Li, H., 2004. Nappe tectonics and their ore-controlling of Lanping basin in Yunnan Province. Geology and Prospecting 40, 7–12 (in Chinese with English abstract).
He, M.Q., Liu, J.J., Li, C.Y., 2004. Metallogenic Mechanisms of Fluids at Large-scale Pb–Zn–Cu Ore Concentrated Area in Lanping Basin: An Example from Baiyangping Cu–Co Polymetallic Deposit. Geological Publishing House, Beijing (in Chinese).
He, L.Q., Song, Y.C., Chen, K.X., Hou, Z.Q., Yu, F.M., Yang, Z.S., Wei, J.Q., Li, Z., Liu, Y.C., 2009. Thrust-controlled, sediment-hosted, Himalayan Zn–Pb–Cu–Ag deposits in the Lanping foreland fold belt, eastern margin of Tibetan Plateau. Ore Geology Reviews 36, 106–132.
Helgeson, H.C., 1969. Thermodynamics of hydrothermal systems at elevated temperatures and pressures. America Journal of Science 267, 729–804.
Hou, Z.Q., Cook, N.J., 2009. Metallogenesis of the Tibetan collisional orogen: a review and introduction to the special issue. Ore Geology Reviews 36, 2–24.
Hou, Z.Q., Ma, H.W., Khin, Z., Zhang, Y.Q., Wang, M.J., Wang, Z., Pan, G.T., Tang, R.L., 2003. The Himalayan Yulong porphyry copper belt: product of large-scale strike-slip faulting in eastern Tibet. Economic Geology 98, 125–145.
Hou, Z.Q., Pan, G.T., Wang, A.J., Mo, X.X., Tian, S.H., Sun, X.M., Ding, L., Wang, E.Q., Gao, Y.F., Xie, Y.L., Zeng, P.S., Qin, K.Z., Xu, J.F., Qu, X.M., Yang, Z.M., Yang, Z.S., Fei, H.C., Meng, X.J., Li, Z.Q., 2006. Metallogenesis in Tibetan collisional orogenic belt: II. Mineralization in late-collisional transformation setting. Mineral Deposits 25, 521–543 (in Chinese with English abstract).
Hou, Z.Q., Khin, Z., Pan, G.T., Mo, X.X., Xu, Q., Hu, Y.Z., Li, X.Z., 2007. Sanjiang Tethyan metallogenesis in S.W. China: tectonic setting, metallogenic epochs and deposit types. Ore Geology Reviews 31, 48–87.
Hou, Z.Q., Song, Y.C., Li, Z., Wang, Z.L., Yang, Z.M., Yang, Z.S., Liu, Y.C., Tian, S.H., He, L.Q., Chen, K.X., Wang, F.C., Zhao, C.X., Xue, W.Z., Lu, H.F., 2008. Thrust-controlled, sediment-hosted Pb–Zn–Ag–Cu deposits in eastern and northern margins of Tibetan orogenic belt: geological features and tectonic model. Mineral Deposits 27, 123–144 (in Chinese with English abstract).
Hu, M.A., 1989a. A preliminary evaluation of the mineralization and their characteristics on the karst-type lead–zinc deposit by the examplification of Jinding, Yunnan Province. Earth Science l4, 53l–538l (in Chinese with English abstract).
Hu, M.A., 1989b. Hydrothermal maturation of indigenous organic matters and their significance in the metallogenic processes of the Jinding lead–zinc deposit, Yunnan Province. Earth Science—Journal of China University of Geosciences 14, 503–512 (in Chinese with English abstract).
Hu, R.Z., Turner, G., Burnard, P.G., Zhong, H., Ye, Z.J., Bi, X.W., 1998. The helium and argon isotopic geochemistry of Jinding super large-scale lead–zinc deposit. Science in China (Series D) 41, 42–48.
Ireland, T.R., 2004. SIMS measurement of stable isotopes. In: de Groot, P. (Ed.), Handbook of Stable Isotope Analytical Techniques, pp. 652–691 (Chapter 30).
Ji, H.B., Li, C.Y., 1998. Geochemical characteristics and source of ore-forming fluid for Jinman copper deposit in western Yunnan Province, China. Acta Mineralogica Sinica 18, 28–37 (in Chinese with English abstract).
Jian, P., Liu, D.Y., Kröner, A., Zhang, Q., Wang, Y.Z., Sun, X.M., Zhang, W., 2009. Devonian to Permian plate tectonic cycle of the Paleo-Tethys orogen in southwest China (I): geochemistry of ophiolites, arc/back-arc assemblages and within-plate igneous rocks. Lithos 113, 748–766.
Jin, X.C., Wang, Y.Z., Xie, G.L., 2003. Devonian to Triassic successions of the Changning–Menglian Belt, Western Yunnan, China. Acta Geologica Sinca 77, 440–456.
Jørgensen, B.B., 1979. A theoretical model of the stable sulfur isotope distribution in marine sediments. Geochimica et Cosmochimica Acta 43, 363–374.
Jørgensen, B.B., Isaksen, M.F., Jannasch, H.W., 1992. Bacterial sulfate reduction above 100 °C in deep-sea hydrothermal vent sediments. Science 258, 1756–1757.
Khin, Z., Peters, S.G., Gromie, P., Burrett, C., Hou, Z.Q., 2007. Nature diversity of deposit types and metallogenic relations of South China. Ore Geology Reviews 31, 3–47.
Kiyosu, Y., Krouse, H.R., 1990. The role of organic acid in the abiogenic reduction of sulfate and the sulfur isotope effect. Geochemical Journal 24, 21–27.
Kozdon, R., Kita, N.T., Huberty, J.M., Fournelle, J.H., Johnson, C.A., Valley, J.W., 2010. In situ sulfur isotope analysis of sulfide minerals by SIMS: precision and accuracy, with application to thermometry of ~3.5 Ga Pilbara cherts. Chemical Geology 275, 243–253.
Kyle, J.K., Li, N., 2002. Jinding: a giant Tertiary sandstone-hosted Zn–Pb deposit, Yunnan, China. SEG Newsletter 50, 8–16.
Layne, G.D., Hart, S.R., Shimizu, N., 1991. Microscale lead and sulfur isotope zonation in hydrothermal sulfides by ion microprobe: new findings from the Mississippi valley-type Pb–Zn deposits of the Viburnum Trend, S.E. Missouri. Geological Society of America Bulletin 23, 101–102.
Leach, D.L., Sangster, D.F., Kelley, K.D., Large, R.R., Garven, G., Allen, C.R., Gutzmer, J., Walters, S., 2005. Sediment-hosted lead–zinc deposits: a global perspective. Economic Geology 100th Anniversary Volume. 561–607.
Lehmann, B., Zhao, X.F., Zhou, M.F., Du, A.D., Mao, J.W., Zeng, P.S., Henjes-Kunst, F., Heppe, K., 2013. Mid-Silurian back-arc spreading at the northeastern margin of Gondwana: the Dapingzhang dacite-hosted massive sulfide deposit, Lancangjiang zone, southwestern Yunnan, China. Gondwana Research 24, 648–663.
Leshin, L.A., McKeegan, K.D., Carpenter, P.K., Harvey, R.P., 1998. Oxygen isotopic constraints on the genesis of carbonates from martian meteorite ALH84001. Geochimica et Cosmochimica Acta 62, 3–13.
Li, N., 1998. Depositional Controls and Genesis of the Jinding Sandstone-hosted Zn–Pb Deposit, Yunnan Province, Southwest China. (Ph.D. thesis) University of Texas at Austin 236.
Li, Y.S., 2002. The Geochemical Studies on Copper Polymetallic Deposits of Middle-southern Part of Lancangjiang, Yunnan Province, China. Hefei University of Technology (Ph.D Dissertation (in Chinese with English abstract)).
Li, N., Kyle, J.K., 1997. Geologic controls of sandstone-hosted Zn–Pb–(Sr) mineralisation, Jinding deposit, Yunnan Province, China—a new environment for sediment-hosted Zn–Pb deposits. In: Pei, R.F. (Ed.), Proceedings, 30th International Geological Congress, 9, pp. 67–82.
Li, Z.M., Liu, J.J., Qin, J.Z., Liao, Z.T., He, M.Q., Liu, Y.P., 2005. Ore-forming material sources of the Baiyangping copper–cobalt–silver polymetallic deposit in Lanping basin, western Yunnan. Geology and Prospecting 41, 1–6 (in Chinese with English abstract).
Li, Y.G., Hou, Z.J., Wang, A.J., Tang, J.X., Liu, J.L., Xue, C.J., Xiu, Q.Y., 2006. Geochemistry of Cenozoic detrital rocks and its constraints on provenance in Lanping basin. Acta Geologica Sinica 22, 751–760 (in Chinese with English abstract).
Liao, Z.T., Chen, Y.K., 2005. Nature and evolution of Lanping–Simao basin prototype. Journal of Tongji University (Nature Science) 33, 1528–1531 (in Chinese with English abstract).
Liu, J.J., Li, C.Y., Zhang, Q., 2001. Wood cell texture from Jinman copper deposit in west Yunnan and its genesis significance. Science in China (Series D) 32, 89–95 (in Chinese with English abstract).
Liu, J.L., Song, Z.J., Cao, S.Y., Zhai, Y.F., Wang, A.J., Gao, L., Xiu, Q.Y., Cao, D.H., 2006. The dynamic setting and processes of tectonic and magmatic evolution of the oblique collision zone between Indian and Eurasian plates: exemplified by the tectonic evolution of the Three River region, eastern Tibet. Acta Petrologica Sinica 4, 755–786 (in Chinese with English abstract).
Liu, J.J., Zhai, D.G., Li, Z.M., He, M.Q., Liu, Y.P., Li, C.Y., 2010. Occurrences of Ag, Co, Bi and Ni elements and its genetic significance in the Baiyangping silver–copper polymetallic motallogenic concentration area, Lanping basin, southwestern China. Acta Petrologica Sinica 26, 1646–1660 (in Chinese with English abstract).
Luo, J.L., Yang, Y.H., Zhao, Z., Chen, J.S., Yang, J.Z., 1994. Evolution of the Tethys in Western Yunnan and Mineralization for Main Metal Deposits. Geological Publishing House, Beijing 157–215 (in Chinese with English abstract).
Machel, H.G., 2001. Bacterial and thermochemical sulfate reduction in diagenetic settings: old and new insights. Sedimentary Geology 140, 143–175.
Machel, H.G., Foght, J., 2000. In: Riding, R. (Ed.), Products and Depth Limits of Microbial Activity in Petroliferous Subsurface Settings. Springer, Berlin.
Machel, H.G., Krouse, H.R., Sassen, R., 1995. Products and distinguishing criteria of bacterial and thermochemical sulfate reduction. Applied Geochemistry 10, 373–389.
McKeegan, K.D., 1987. Oxygen isotopes in refractory stratospheric dust particles: proof of extraterrestrial origin. Science 237, 1468–1471.
McKibben, M.A., Eldridge, S.C., 1995. Microscopic sulfur isotope variations in ore minerals from the Viburnum Trend, Southeast Missouri: a SHRIMP study. Economic Geology 90, 228–245.
Merce, C., Carlos, A., Esteve, C., 2004. Hydrothermal mixing, carbonate dissolution and sulfide precipitation in Mississippi Valley-type deposits. Mineralium Deposita 39, 344–357.
Metcalfe, I., 2006. Palaeozoic and Mesozoic tectonic evolution and palaeogeography of East Asian crustal fragments: the Korean Peninsula in context. Gondwana Research 9, 24–46.
Metcalfe, I., 2011. Tectonic framework and Phanerozoic evolution of Sundaland. Gondwana Research 19, 3–21.
Misra, K.C., 2000. Understanding Mineral Deposits. Kluwer Academic Publishers, London 845.
Mu, C.L., Wang, J., Yu, Q., Zhang, L.S., 1999. The evolution of the sedimentary basin in Lanping area during Mesozoic–Cenozoic. Journal of Mineralogy and Petrology 19, 30–36 (in Chinese with English abstract).
Neal, C.R., Davidson, J.P., McKeegan, K.D., 1995. Geochemical analysis of small samples: micro-analytical techniques for the nineties and beyond. Reviews of Geophysics 25–32.
Ohmoto, H., 1972. Systematics of sulfur and carbon isotopes in hydrothermal ore deposits. Economic Geology 67, 551–578.
Ohmoto, H., 1992. Biogeochemistry of sulfur and the mechanisms of sulfide–sulfate mineralization in Archean oceans. In: Schidlowski, M., Golubic, S., Kimberley, M.M., McKirdy, D.M., Trudinger, P.A. (Eds.), Early Organic Evolution, Implications for Mineral and Energy Resources. Springer-Verlag, pp. 378–397.
Ohmoto, H., Rye, R.O., 1979. Isotopes of sulfur and carbon. In: Barnes, H.L. (Ed.), Geochemistry of Hydrothermal Ore Deposits. Wiley, New York, pp. 509–567.
Olson, R.A., 1984. Genesis of paleokarst and strata-bound zinc–lead sulfide deposits in a Proterozoic dolostone, northern Baffin Island, Canada. Economic Geology 79, 1056–1103.
Orr, W.L., 1974. Changes in sulfur content and isotopic ratios of sulfur during petroleum maturation—study of Big Horn Basin Paleozoic oils. AAPG Bulletin — American Association of Petroleum Geologists 58, 2295–2318.
Peevler, J., Fayek, M., Misra, K.C., Riciputi, L.R., 2003. Sulfur isotope microanalysis of sphalerite by SIMS: constraints on the genesis of Mississippi valley-type mineralization, from the Mascot-Jefferson City district, East Tennessee. Journal of Geochemical Exploration 80, 277–296.
Qin, G.J., Zhu, S.Q., 1991. The ore-forming model of the Jinding lead–zinc deposit and prediction. Yunnan Geology 10, 145–190 (in Chinese with English abstract).
Reed, S.J.B., 1989. Ion microprobe analysis—a review of geological applications. Mineralogical Magazine 53, 3–24.

Reed, S.J.B., 1990. Recent developments in geochemical microanalysis. Chemical Geology 83, 1–9.
Rees, C.E., 1973. A steady-state model for sulphur isotope fractionation in bacterial reduction processes. Geochimica et Cosmochimica Acta 37, 1141–1162.
Riciputi, L.R., Paterson, B.A., Ripperdan, R.L., 1998. Measurement of light stable isotope ratios by SIMS: matrix effects for oxygen, carbon, and sulfur isotopes in minerals. International Journal of Mass Spectrometry 178, 81–112.
Sakai, H., 1968. Isotopic properties of sulfur compounds in hydrothermal processes. Geochemical Journal 2, 29–49.
Sangster, D.F., 1990. Mississippi Valley-type and Sedex lead–zinc deposits — a comparative examination. Institution of Mining and Metallurgy Transactions Section B: Applied Earth Sciences 99, 21–42.
Scotese, C.R., 2000. Paleomap projects. http://www.scotese.com/earth.htm2000.
Sengor, A.M.S., 1985. The story of Tethys: how many wives did okeanos have? Episodes 8, 3–12.
Shi, J.X., Yi, F.H., Wen, Q.D., 1983. The rock-ore characteristics and mineralization of Jinding lead–zinc deposit, Lanping. Yunnan Geology 2, 179–195 (in Chinese with English abstract).
Spurlin, M.S., Yin, A., Horton, B.K., Zhou, J.Y., Wang, J.H., 2005. Structural evolution of the Yushu–Nangqian region and its relationship to syncollisional igneous activity, eastcentral Tibet. GSA Bulletin 117, 1293–1317.
Sverjensky, D.A., 1981. The origin of a Mississippi valley-type deposit in the Viburnum Trend, Southeast Missouri. Economic Geology 76, 1848–1872.
Tang, Y.Y., Bi, X.W., He, L.P., Wu, L.Y., Feng, C.X., Zou, Z.C., Tao, Y., Hu, R.Z., 2011. Geochemical characteristics of trace elements, fluid inclusions and carbon–oxygen isotopes of calcites in the Jinding Zn–Pb deposit, Lanping, China. Acta Petrologica Sinica 27, 2635–2645 (in Chinese with English abstract).
Tao, X.F., Zhu, L.D., Liu, D.Z., Wang, G.Z., Li, Y.G., 2002. The formation and evolution of the Lanping basin in western Yunnan. Journal of Chengdu University of Technology 29, 521–525 (in Chinese with English abstract).
Thamdrup, B., Finster, K., Hansen, W., Bak, F., 1993. Bacterial disproportionation of elemental sulfur coupled to chemical reduction of iron and manganese. Applied and Environmental Microbiology 59, 101–108.
Third Geological Team, 1984. The exploration report of the Jinding Zn–Pb deposit in Lanping County, Yunnan Province. Yunnan Bureau of Geology and Mineral Resources 50–106 (in Chinese).
Veevers, J.J., 2006. Updated Gondwana (Permian–Cretaceous) earth history of Australia. Gondwana Research 9, 231–260.
Veevers, J.J., 2009. Palinspastic (pre-rift and -drift) fit of India and conjugate Antarctica and geological connections across the suture. Gondwana Research 16, 90–108.
Wagner, T., Okrusch, M., Weyer, S., Lorenz, J., Yann, L., Taubald, H., Schmitt, R.T., 2010. The role of the Kupferschiefer in the formation of hydrothermal base metal mineralization in the Spessart ore district, Germany: insight from detailed sulfur isotope studies. Mineralium Deposita 45, 217–239.
Wang, J.H., Yin, A., Harrison, T.M., Grove, M., Zhang, Y.Q., Xie, G.H., 2001. A tectonic model for Cenozoic igneous activities in the eastern Indo-Asian collision zone. Earth and Planetary Science Letters 188, 123–133.
Wang, F., He, M.Y., 2003. Lead and sulfur isotopic tracing of the ore-forming material from the Baiyangping copper–silver polymetallic deposit in Lanping, Yunnan. Sedimentary Geology and Tethyan Geology 23, 82–85 (in Chinese with English abstract).
Wang, A.J., Cao, D.H., Gao, L., Wang, G.S., Guan, Y., Xiu, Q.Y., Liu, J.L., 2009. A probe into the genesis of Jinding super-large Pb–Zn ore deposit. Acta Geologica Sinica 83, 43–54 (in Chinese with English abstract).
Wang, X.H., Song, Y.C., Hou, Z.Q., Zhang, H.R., Liu, Y.C., Yang, Z.S., Yang, T.N., Pan, X.F., Wang, S.X., Xue, C.D., 2011. Characteristics of trace elements and S–Pb isotopes in sphalerites from lead–zinc polymetallic deposits in Fulongchang area, Lanping Basin, western Yunnan Province, and their implications. Acta Petrologica et Mineralogica 30, 45–59 (in Chinese with English abstract).
Warren, J.K., 1999. Evaporites: Their Evolution and Economics. Blackwell Scientific Publication, Oxford.
Wei, J.Q., 2001. Pb–S isotopic geochemistry of copper multi-metal deposits in Hexi, Yunnan Province. Geology and Mineral Resource of South China 36–39 (in Chinese with English abstract).
Wen, C.Q., Cai, J.M., Liu, W.Z., Tan, G.J., Chen, S.F., 1995. Geochemical characteristics of fluid inclusions of the Jinding lead–zinc deposit, Yunnan, China. Journal of Mineralogy and Petrology 15, 78–84 (in Chinese with English abstract).
Xu, Q.D., Li, J.W., 2003. Migration of ore-forming fluids and its relation to zoning of mineralization in northern Lanping Cu-polymetallic area, Yunnan Province: evidence from fluid inclusions and stable isotopes. Mineral Deposits 22, 366–376 (in Chinese with English abstract).
Xu, Q.D., Zhou, L., 2004. Ore-forming fluid migration in relation to mineralization zoning in Cu-polymetallic mineralization district of northern Lanping, Yunnan: evidence from Lead isotope and mineral chemistry of ores. Mineral Deposits 23, 452–463 (in Chinese with English abstract).
Xue, C.J., Wang, D.H., Chen, Y.C., Yang, J.M., 2000. Helium, argon, and xenon isotopic compositions of ore-forming fluids in Jinding–Baiyangping polymetallic deposits, Yunnan, Southwest China. Acta Geologica Sinica 74, 521–528.
Xue, C.J., Chen, Y.C., Yang, J.M., Wang, D.H., 2002. Jinding Pb–Zn deposit: geology and geochemistry. Mineral Deposits 21, 270–277 (in Chinese with English abstract).
Xue, C.J., Chen, Y.C., Wang, D.H., Yang, J.M., Yang, W.G., 2003. Geology and isotopic composition of helium, neon, xenon and metallogenic age of the Jinding and Baiyangping ore deposits, northwest Yunnan, China. Science in China (Series D) 46, 789–800.
Xue, C.J., Zeng, R., Gao, Y.B., Zhu, H.P., Zhao, S.H., Li, Y.Q., 2006. Fluid processes of a heavy metallogenesis at Jinding, Lanping, SW-China. Acta Petrologica Sinica 22, 1031–1039 (in Chinese with English abstract).
Xue, C.J., Gao, Y.B., Zeng, R., Chi, G.X., Qing, H.R., 2007a. Organic petrography and geochemistry of the Giant Jinding deposit, Lanping basin, northwest Yunnan, China. Acta Petrologica Sinica 23, 2889–2900 (in Chinese with English abstract).
Xue, C.J., Zeng, R., Liu, S.W., Chi, G.X., Qing, H.R., Chen, Y.C., Yang, J.M., Wang, D.H., 2007b. Geologic, fluid inclusion and isotopic characteristics of the Jinding Zn–Pb deposit, western Yunnan, South China: a review. Ore Geology Reviews 31, 337–359.
Xue, C.J., Gao, Y.B., Chi, G.X., David, L.L., 2009. Possible former oil–gas reservoir in the giant Jinding Pb–Zn deposit, Lanping, NW-Yunnan: the role in the ore accumulation. Journal of Earth Science and Environment 31, 221–229 (in Chinese with English abstract).
Yan, W., Li, Z.Y., 1997. Geochemical characteristics and their hydrothermal sedimentary genesis of a new type of copper deposit. Geochimica 26, 54–63 (in Chinese with English abstract).
Yang, W.G., Yu, X.H., Li, W.C., Dong, F.L., Mo, X.X., 2003. The characteristics of metallogenic fluids and metallogenic mechanism in Baiyangping copper and polymetallic mineralization concentration area in Yunnan Province. Geoscience 17, 27–33 (in Chinese with English abstract).
Ye, Q.T., Hu, Y.Z., Yang, Y.Q., 1992. Regional Geochemistry Background and the Gold–Silver–Lead–Zinc Mineralization in Sanjiang Area. Geological Publishing House, Beijing 21–264 (in Chinese).
Yin, A., Harrison, T.M., 2000. Geologic evolution of the Himalayan–Tibetan orogen. Annual Review of Earth and Planetary Sciences 28, 211–280.
Yin, H.H., Fan, W.M., Lin, G., 1990. The deep factor of geodepression basin evolution and the mineralization of crust–mantle mixing in Lanping–Simao, Yunnan. Tectonics and Metallogenic Geology 14, ll3–l24 (in Chinese with English abstract).
Yu, X.Q., Wu, G.G., Zhao, X.X., Zhang, D., Di, Y.J., Qiu, J.T., Dai, Y.P., Li, C.L., 2012. New geochronological data from the Paleozoic and Mesozoic nappe structures, igneous rocks, and molybdenite in the North Wuyi area, Southeast China. Gondwana Research 22, 519–533.
Zeng, R., 2007. The Large Scale Fluid Ore-forming Process in the Lanping Basin—Taking the Jinding and Baiyangping Deposits as the Examples. (Dissertation for Doctoral Degree) Chang'an University, Xi'an (in Chinese).
Zhang, J.R., Wen, H.J., 2012. Sulfur and lead isotope compositions and tracing of copper deposits on the western border of the Lanping Basin, Yunnan Province. Geochemica 41, 166–180 (in Chinese with English abstract).
Zhang, C.J., Ni, S.J., Teng, Y.G., Peng, X.H., Liu, J.D., 2000. Relationship between Himalayan tecotonomagmatic movement and mineralization in Lanping basin, Yunnan Province. Journal of Mineralogy and Petrology 20, 35–39 (in Chinese with English abstract).
Zhao, X.Y., 1989. On the genesis of the Jinding lead–zinc ore deposit in Yunnan. Earth Science 14, 523–530 (in Chinese with English abstract).
Zhao, H.B., 2006. Study on the Characteristics and Metallogenic Conditions of Copper-polymetallic Deposits in Middle-northern Lanping Basin, Western Yunnan. (Dissertation for Doctoral Degree) China University of Geosciences, Beijing (in Chinese).
Zhong, D.L., Ding, L., Liu, F.T., Liu, J.H., Zhang, J.J., Ji, J.Q., Chen, H., 2000. Poly-layered architecture of lithosphere in orogen and its constraint on Cenozoic magmatism example from Sanjiang and surrounding area. Science in China (Series D) 30 (S1), 1–8 (in Chinese with English abstract).
Zhou, W.Q., Zhou, Q.L., 1992. A study on the isotope composition of Pb and S in the Lanping Pb–Zn deposit, Yunnan Province. Geochimica 2, 141–148 (in Chinese with English abstract).